9 Longwave passive remote sensing

Clémence Pierangelo
Contributions from Alain Chédin, Michel Legrand

9.1 Introduction

The longwave spectral domain dealt with here, also called the "thermal infrared" domain, roughly covers the 3–15 μm spectral range. The main radiation source is not the sun but the Earth system, that is, the Earth's surface (land and ocean) and the atmosphere. The infrared emission from bodies is directly linked to their temperature as described by Plank's law: the hotter the bodies are, the higher their emission. The Earth and its atmosphere are heated by the fraction of sunlight they absorb. Their increase in temperature results in increased infrared emission to space, thus ensuring the energy balance of the Earth system.

The exact ranges of spectral domains are the subject of frequent discussion. To avoid any confusion, we hereby give the definitions that apply in this chapter:

- The word "longwave" applies to the thermal radiation emitted by the Earth system. Thus, it goes practically from 3 to 25 μm.
- The word "shortwave" applies to the radiation emitted by the sun. For satellite nadir observation, it roughly goes up to 4 μm. Beyond this wavelength, the shortwave contribution turns to be negligible in comparison with the longwave one. But for satellite limb observations or solar occultation, the shortwave radiation might be not negligible at higher wavelengths[1].

1 The infrared emission spectrum of the Earth goes up to 1000 μm. Between 25 and 1000 μm, the far-infrared is not useful for remote sensing applications as the atmosphere becomes opaque. Beyond 1 mm, the radiation emitted by the Earth is in the microwave domain and does not interact with aerosols as particle size is too low, with respect to the wavelength.

J. Lenoble et al. (eds.), *Aerosol Remote Sensing*, Springer Praxis Books,
DOI 10.1007/978-3-642-17725-5_9, © Springer-Verlag Berlin Heidelberg 2013

However, not all the longwave domain is relevant for remote sensing applications: the totally opaque spectral ranges due to strong gaseous absorption bands must be avoided. Therefore, only the 3–15 μm spectral range is of interest here. In this spectral domain both "longwave" and "shortwave" radiation (by day only for the latter) are to be considered:

- The "medium infrared" range, roughly corresponding to the 3–4 μm range, is characterized by the contribution of both shortwave and longwave radiations.
- The "thermal infrared" range, corresponding to the 4–15 μm range and including the 10-μm atmospheric window, is the domain of the longwave radiation.

Several interactions can occur between the electromagnetic field, the Earth's surface, and the molecules and particles of the atmosphere. The infrared radiation emitted by the Earth's surface and by the atmosphere can be absorbed, scattered, and emitted, by the aerosol. Compared to shorter wavelengths, the specificity of the longwave domain regarding aerosols lies in the emission process.

Moreover, in the thermal infrared, many atmospheric gases (CO_2, H_2O, ozone, etc.) have strong absorption lines, caused by the rotation and vibration of atoms inside the molecules. Most of the spectrum in the infrared is then affected by gaseous absorption and emission; consequently, this feature must be taken into account when building up a retrieval of aerosol properties.

The heating and cooling effects of the aerosols result from their combined interaction with longwave and shortwave radiations. In the longwave, a non-negligible part of the radiation upwelling from the surface is absorbed and scattered by the particles. The radiation is then re-emitted, partly downwards, and also back-scattered towards the Earth's surface. Thus, the aerosols in the thermal infrared produce a greenhouse effect in the lower atmosphere and a surface heating. This effect is the opposite of the direct radiative effect observed in the shortwave resulting in a surface cooling. During daylight, the shortwave effect is prevailing and the aerosol presence results in a surface cooling, whilst at night it results in a surface heating. A short review of the literature shows that the direct radiative forcing in the longwave domain is far from negligible (Markowicz et al., 2003; Vogelman et al., 2003). However, the domain remains largely unexplored and is poorly understood. Coordinated research strategies for its study are thus recommended (Yu et al., 2006).

The longwave radiation primarily depends on the characteristics of the Earth's surface (temperature and emissivity), on the thermodynamic state of the atmosphere (temperature and humidity profiles), and on its chemical and mineral composition, including the aerosols. These coupled dependencies are one of the main difficulties when using thermal radiation for aerosol remote sensing. However, longwave remote sensing of particles offers some unique possibilities, such as night-time aerosol observations, the retrieval of the aerosol layer altitude or dust detection over deserts. Besides, aerosol effects on the infrared radiance must be taken into account for other retrievals using the infrared spectrum. For instance, the retrievals of the temperature and moisture profiles, used for weather forecasts, are affected by the presence of dust, as shown by Weaver et al. (2003).

Note about the units: when dealing with high resolution spectra, often recorded by a Fourier Transform spectrometer, the gaseous spectroscopy is of first significance. Thus, because of the way this instrument concept records the spectrum and because of the spec-

troscopy habits, the wavenumber (in cm^{-1}) is a more natural unit than the wavelength (in μm). On the other hand, when dealing with aerosol optical properties, the wavelength is more appropriate because these properties depend on the ratio of the particle size to the wavelength. Consequently, we keep both units hereafter, and a conversion scale is given at the end of the chapter.

In this chapter, we first focus on the aerosol optical properties in the longwave domain, and on their significant consequences on the remote sensing validity domain and strategy. Then, the radiative transfer equation in the thermal infrared is specifically studied, including the scattering contribution by aerosols. Next, we review the techniques and algorithms currently used for aerosol detection and remote sensing in the longwave, including the pre-processing steps of cloud clearing. Finally, some illustrations of experimental results are given, obtained both from satellite sensors (sounders and imagers) and from ground-based instruments.

9.2 Aerosol optical properties in the longwave domain

As the definition and the modeling of aerosol optical properties (absorption and scattering) have previously been described in this book (see Chapter 2), we focus here on the specificity of the longwave domain.

9.2.1 On the relative impact of aerosol species in the infrared

Before studying the effect of the microphysical properties of aerosols on their infrared optical properties in more detail, we first examine the relative impact of the main aerosol species. For the optical remote sensing of aerosols, the variable of prime interest is optical depth, as it combines both the information on the columnar amount of aerosols (number of particles, mass, etc.) and the optical extinction efficiency factor (i.e. the strength with which the aerosol interacts with the radiation, by scattering or absorbing the photons). The optical depth at a given wavelength is usually the quantity observed by a passive remote sensor recording the radiation at this given wavelength. However, the optical depth is strongly dependent on the wavelength. This is why the primary quantity that may be retrieved from measurements in the longwave domain is the AOD at infrared wavelengths (and not at some visible wavelength). Nevertheless, most aerosol observations are performed in the visible or near-infrared domain: generally, the 0.55 μm wavelength is taken as a reference. This is why we might estimate the relative impact of aerosol species in the infrared by comparing their infrared AOD to their visible AOD, or, equivalently, their infrared extinction coefficient to their visible extinction coefficient.

The ratio of infrared to visible optical depths (normalized at 0.55 μm), at wavelengths from 4 to 12 μm, for several aerosol species shows a high variability of aerosol type (see Figure 9.1: aerosol types are taken from the OPAC – Optical Properties of Aerosol and Clouds database from Hess et al. (1998)). Consequently, this high variability implies that the longwave and shortwave remote sensing observations are not sensitive to the same aerosol types. One of the main reasons why some aerosols are optically thick and others have

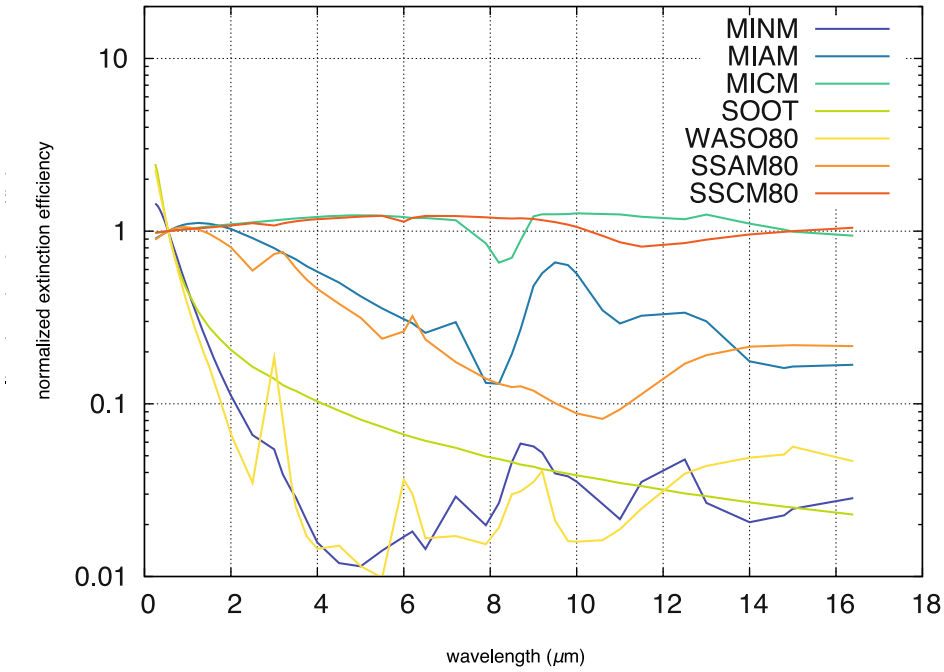

Figure 9.1 Normalized extinction coefficient as a function of wavelength for 7 types of aerosol component, taken from the OPAC database (Hess et al., 1998) (MINM=Mineral Nucleus Mode, MIAM=Mineral Accumulation Mode, MICM=Mineral Coarse Mode, WASO80=Water Soluble, 80% humidity, SOOT=soot, SSAM80= Sea-Salt Accumulation Mode 80% humidity, SSCM80=Sea-Salt Coarse Mode 80% humidity). The normalization is performed at 0.55 μm.

almost no effect in the infrared is their size distribution, as will be explained in more detail in Section 9.2.3. As an illustration, it can be seen on Figure 9.1 that aerosols in the coarse mode have the highest impact in the infrared (e.g. mineral aerosols or sea-salt in coarse mode). Amongst tropospheric aerosols, it is dust that has the main impact in the infrared. Indeed, aerosol types which are more typical of pollution or biomass burning (such as water-soluble aerosol or soot on Figure 9.1) are usually smaller in size. The optical depth of sea-salt in coarse mode is not negligible either. However, sea-salt particles are usually confined to the bottom of the planetary boundary layer, which prevents them from having an impact on radiance collected at satellite level, as will be explained in Section 9.3.6. Mineral dust aerosol is firstly mainly composed of particles in coarse size mode, potentially promoting a high infrared optical depth, and secondly can reach high altitudes, for example in the so-called Saharan-boundary layer (Chiapello et al., 1995). Subsequently, the remote sensing of aerosols in the longwave domain will mostly focus on retrievals of mineral dust properties.

Another serious consequence of these considerations is that there is no point in trying to retrieve visible optical depth from infrared observations, unless some other *a priori* information is available. Indeed, there is no unique relationship between the directly observable (the infrared optical depth) and the visible optical depth, but many possibilities depending on the aerosol type and size mode. This also implies that the validation of infrared optical depth with visible observations is difficult and limited.

Let us also mention volcanic aerosol. There are two types of volcanic aerosol: ash particles in the troposphere and sulfuric acid droplets in the stratosphere. Volcanic ash is emitted in great quantities during extreme events and has a lifetime of a few days in the troposphere. It contains particles in the 10 μm size range which have an effect on infrared observations. The stratospheric aerosol consists of sulfuric acid droplets (H_2SO_4) transformed from SO_2 emitted by volcanic eruptions (e.g. El Chichon or Pinatubo eruptions) into aerosol through gas-particle conversions. Although their infrared optical depth is below 0.1, they can be detected by infrared sensors, thanks to their global distribution, their long life in the stratosphere (several months or even years) and their high altitude (see Section 9.5.1 for an illustration).

9.2.2 Effect of refractive indices (or composition)

The chemical or mineralogical composition of aerosol is represented in its optical properties through the real and imaginary parts of its refractive index at every wavelength. The composition of aerosol is highly variable, depending on the source location, the emission process and the atmospheric conditions. Aerosol particles, and especially mineral aerosols, are generally composed of a mixture of mineral and/or carbonaceous elements that can be internally mixed or more often externally mixed (Chou et al., 2008). Therefore, the refractive index is one of the lesser-known quantities when computing the optical properties of aerosols in the infrared. Indeed, most studies have focused on the visible refractive index (e.g. McConnell et al, 2010).

Two different approaches are possible to obtain refractive indices of aerosols. The first one consists of taking values measured from real atmospheric aerosol particles, whereas the second consists of combining values from elementary components (or minerals for dust aerosols) in order to obtain the refractive indices of the mixture (following the approach of Sokolik and Toon, 1999, for example). The advantages of the second method are the availability of data (numerous measurements from soil samples, however not globally distributed), and the possibility of relating various minerals and particle size modes, while the difficulty lies in the modelling of the mixture.

Amongst one of the first inventories of refractive indices of aggregated particles, Volz (1973) published a dataset of refractive indices in the infrared for various kinds of aerosol: Saharan dust, volcanic dust, coal-fire fly ash and ammonium sulphate droplets. Concerning mineral dust, Sokolik et al. (1998) list the measurements performed in the infrared range (see their Table 1) and previously published in Volz (1972, 1973), Fischer (1976), Patterson (1981), Fouquart et al. (1987) or Sokolik and Golitsyn (1993). Each dataset comes from aerosols collected on a regional scale only and cannot thus be applied worldwide. For example, no measurements from Asian dust are available so far. Sokolik et al. (1998) note that the only measurements of dust particles far from the aerosol sources are the measure-

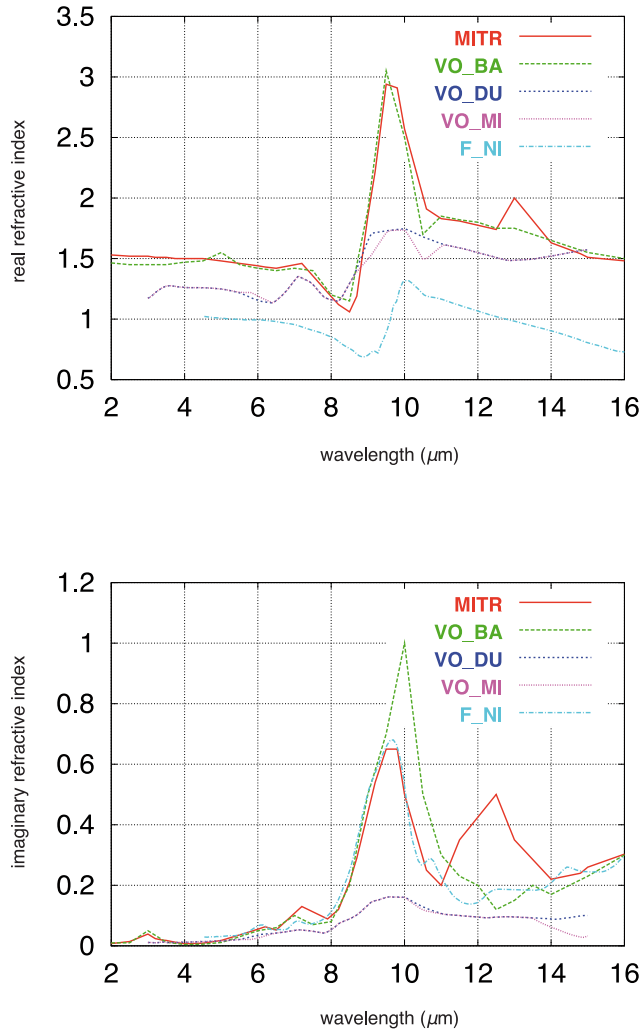

Figure 9.2 Refractive index of 5 mineral dust aerosol data set: MITR=Mineral Transported aerosol from Carlson and Benjamin (1980) and Sokolik et al. (1993), VO_BA=Saharan dust aerosol at Barbados (Volz, 1973), VO_DU=continental dust in Germany (Volz, 1973), VO_MI=mineral aerosol in Germany (Volz, 1973), F_NI=Saharan dust aerosol above Niger (Fouquart, 1987) from 4.5 to 16 μm. Real part (top) and absolute value of imaginary part (bottom).

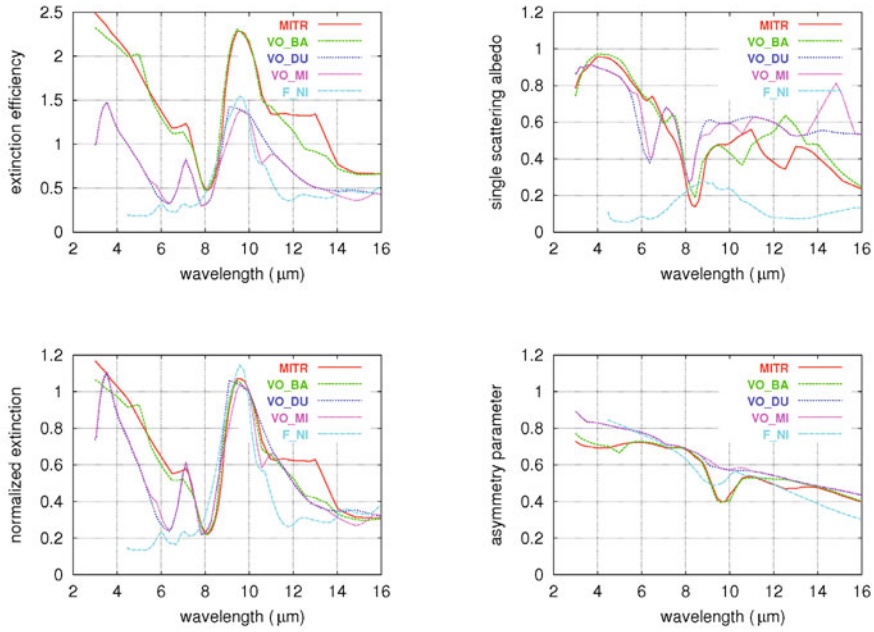

Figure 9.3 Effect of the refractive indices of mineral dust on the optical properties for 5 data sets for a Mie calculation. See legend in Figure 9.2 for the meaning of the data set.

ments from Volz (1973). The remote sensing of aerosols from space requires knowledge of aerosols on a global scale, especially concerning those far from their sources. This is why, following Sokolik et al. (1998), we recommend the indices from Volz (1973) for remote sensing of Saharan aerosols far from their sources. The "Mineral Transported" model from the OPAC database mentioned above is similar to, indeed is mainly based on, the Volz (1973) indices slightly modified by Carlson and Benjamin (1980). As an example Figure 9.2 illustrates the great variability of dust refractive indices as a function of wavelength. These spectral features are strongly dependent on the minerals that constitute the aerosol (see below). The variability between aerosol sources is also very great, in particular between desert sources and continental sources, and this greatly affects the optical properties important for radiative transfer (see Figure 9. 3), in agreement with Highwood et al. (2003). The composition of aerosols also changes during transport, as can be seen by comparing refractive indices for Saharan dust over Niger or Barbados.

Since the variability of soil minerals is very high, Claquin et al. (1999) have chosen a mineralogical set adapted to aerosol remote sensing, based on the abundance, optical prop-

erties and chemical properties of minerals. The study of refractive indices cannot be performed without taking into account the size distribution of particles, as minerals do not all appear in the same particle size range (e.g. Claquin et al, 1999). Their final set consists of eight major minerals: illite, kaolinite and smectite in the clay fraction, and calcite, quartz, feldspar, hematite and gypsum in the silt fraction. The refractive indices of illite, kaolinite, smectite and feldspar (which are all aluminosilicates) are not significantly different, and finally, the variability of refractive indices of dust species is summarized by quartz, clay (and feldspar), calcite and hematite. Similarly, Sokolik and Toon (1999) examined the refractive indices of seven minerals (illite, kaolinite, montmorillonite, hematite, quartz, calcite and gypsum), and they ended up with three main classes relevant to the modeling of aerosol optical properties: clays, quartz and hematite. Others, such as Chou et al. (2008), made in-situ observations that could sum up the variability of dust to aluminosilicates (illite and kaolinite), quartz and iron oxide (i.e. hematite and goethite). The mineralogical species to be considered must also be adapted to the spectral domain of the observation instrument. For instance, Turner (2008) worked on the 8–13 μm domain and, according to the signatures of minerals in this spectral domain, he considered three main minerals that have distinctly

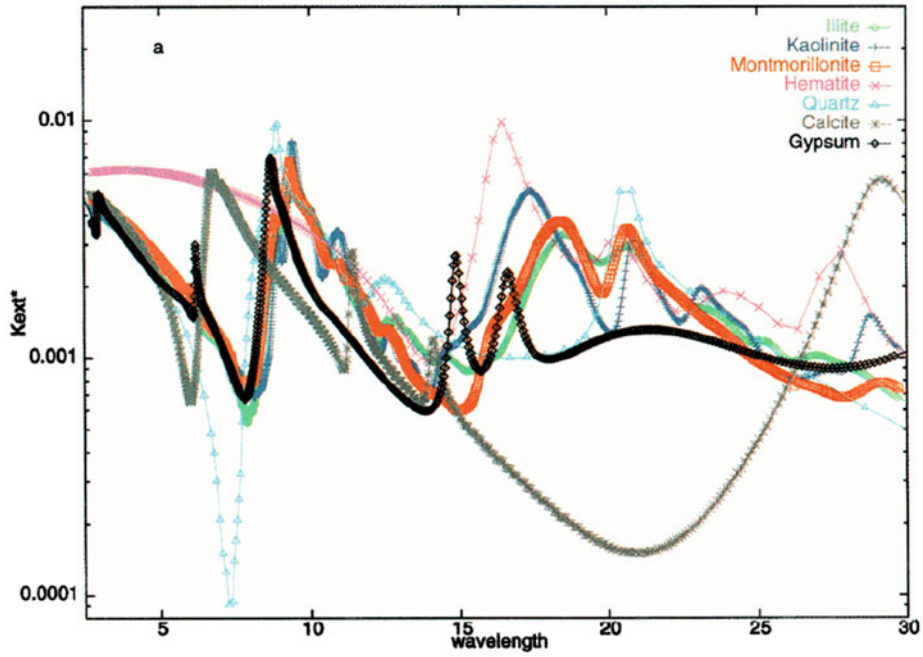

Figure 9.4 Spectral extinction coefficient for individual minerals (normalized for 1 particle per cm^{-3}), computed for a lognormal size distribution with mode radius=0.5 μm and width=2; from Sokolik and Toon (1999).

different absorption bands: kaolinite, gypsum and quartz. The exact minerals in hand must also be adapted to the region of observations (e.g. Hansell et al., 2008).

The description of the main spectral features of each mineral is outside the scope of this chapter and we therefore refer readers interested in this subject to the paper from Sokolik and Toon (1999) and its references. To sum up, the spectral peaks in the extinction efficiency are caused by high imaginary indices, related to absorption of light by stretching vibrations of molecules. For instance, quartz has a major absorption line at 9.2 μm due to Si-O-Si asymmetric stretching vibrations. More generally, silicates show this spectral feature between 8 and 12 μm as the vibration line can be shifted in presence of other ions in the crystal lattice (Al, water, hydroxyl, etc.), whereas calcite exhibits a strong line at 7 μm and weak lines between 11.4 and 14.3 μm, and gypsum shows spectral lines near 8.7 and 16 μm (Sokolik et al., 1998). The great variability of spectral features for pure minerals is shown in Figure 9.4, taken from Sokolik and Toon (1999). Obviously, the extinction maximum between 9 and 10 μm typical of quartz and clays is also visible in the spectrum obtained from aggregated aerosols, as plotted in Figure 9.3.

An updated list of refractive index measurements available in the infrared domain for 7 minerals is given in Balkanski et al. (2007), together with the spectral domain covered by each measurement. It can be noted that very few refractive index spectra cover both the visible and infrared domains. This explains why the extrapolation of infrared optical depth or radiative forcing from only visible measurements requires many assumptions and results in great uncertainties.

9.2.3 Effect of size distribution

The particle size distribution (PSD) of aerosols, and particularly of dust, is often bimodal, as shown by Dubovik et al. (2002). So, as the interaction between light and a particle reaches its maximum when wavelength and size are of the same order of magnitude (see Chapter 2), it is mainly the coarse mode that has an impact on the thermal infrared radiation.

Let us consider the example of a typical size distribution retrieved from AERONET over Capo Verde in April 2003 (http://aeronet.gsfc.nasa.gov/). It can be modeled by a bimodal lognormal volumic size distribution (see Chapter 1) characterized by its modal volumic radii r_{vi} and widths σ_{vi} for mode i:

$$r_{vf}=0.138\ \mu\text{m}, \ln(\sigma_{vf})=0.508;$$
$$r_{vc}=2.00\ \mu\text{m}, \ln(\sigma_{vc})=0.608;$$

where the subscripts v, f and c mean "volumic", "fine mode", and "coarse mode".

The volume of dust in the fine (respectively coarse) mode is V_f, (respectively V_c). The size distribution retrieved by the AERONET sun-photometer also provides the ratio $V_c/V_f=2.71$.

A Lorenz-Mie calculation based on these data and the refractive indices of mineral aerosols in the OPAC database, using the code available at ftp://ftp.giss.nasa.gov/pub/crmim/spher.f (Mishchenko et al., 2002), gives the extinction coefficients for the fine and coarse modes in Table 9.1. The extinction efficiency, or efficiency factor for extinction, Q_{ext}, is

defined here as the ratio of the mean extinction cross-section per particle by the mean surface area per particle, consistently with Chapter 2.

For dust with a typical bimodal distribution, the fine mode contribution to the total optical depth at 10 μm is usually of the order of 10%. This differs from the visible domain where the fine mode is predominant. We can therefore assert one of the main conclusions of this chapter: even for the same aerosol species, the infrared and visible AOD cannot be compared directly; their ratio obviously depends on the relative abundance between fine and coarse particles. However, the comparison of both products contains some valuable information on dust size distribution. A second consequence is that making the approximation of a monomodal lognormal particle size distribution (PSD) is acceptable, since these simulations demonstrate that the contribution of the accumulation mode to the total optical depth is of the order of 10%. Indeed, infrared radiation mostly interacts with coarse mode particles.

This makes it possible to reduce the number of parameters of the PSD to just one: the coarse mode effective radius (see Chapter 1), which is the most significant size parameter in terms of radiative impact. Indeed, the effective radius is well suited to describe the effect of size on optical properties (Mishchenko et al., 2002) while the PSD width (its geometric standard deviation) has a weak effect with regard to its range of variation. For instance, the impact of the geometric standard deviation of the PSD (in the range 1.6 to 2.5) on the normalized extinction coefficient between 3.8 and 15 μm is below 10%. The geometric standard deviation of the distribution is hereafter fixed at 2.2, in agreement with in-situ measurements reported by Reid et al. (2003).

The impact of the effective radius on optical properties (extinction, single scattering albedo, asymmetry parameter) is computed with the above-mentioned Lorentz-Mie code (Mishchenko et al., 2002) and plotted from 3 to 16 μm on Figure 9.5. At first glance, the impact of the effective radius on extinction efficiency seems huge. However, this effect depends slightly on the wavelength, as can be seen on the plot of the extinction efficiency normalized at 10 μm. It is worth pointing out that the radiation at satellite level does not solely depend on the extinction efficiency Q (or extinction cross-section C), but rather on the vertically integrated extinction coefficient (i.e. the optical depth), that is the product of the extinction cross-section to the particle number. An aerosol layer with extinction cross-section C and particle number N or an aerosol layer with extinction cross-section C/2 and particle number 2N are indeed strict equivalents with regard to the measurement. The particle number or concentration is usually totally unknown, because it is the optical depth that is directly measured. We will show through the radiative transfer equation in Section 9.3 that a single channel retrieval algorithm cannot distinguish between N and C without *a priori* information. A multispectral retrieval algorithm requires knowledge of optical depth at every channel frequency τ_{v0}, τ_{v1}, τ_{v2}, etc. Once a reference frequency ν_0 has been chosen, this is equivalent to knowledge of τ_{v0}, C_{v1}/C_{v0}, C_{v2}/C_{v0}, etc. Consequently, for a given optical depth at a given wavelength, only the spectral variations of the extinction cross-section can modify the effect of aerosol on the observation. We call "normalized extinction" the ratio between extinction cross-section at wavelength λ and at a reference wavelength λ_0, usually 10 μm here. This is why we focus on the normalized extinction (and not the extinction efficiency) when evaluating the impact of a microphysical property on optical properties. Going back to Figure 9.5, the effective radius moderately modifies the

Wavelength (μm)	Fine mode		Coarse mode	
	Extinction efficiency	AOD contribution	Extinction efficiency	AOD contribution
0.55	1.957E-2	0.793	6.7662	0.207
10	6.749E-4	0.137	5.6373	0.863

Table 9.1 Contributions of the fine and coarse modes of a bimodal size distribution of mineral dust aerosol on the total optical depth, at 0.55 μm and 10 μm

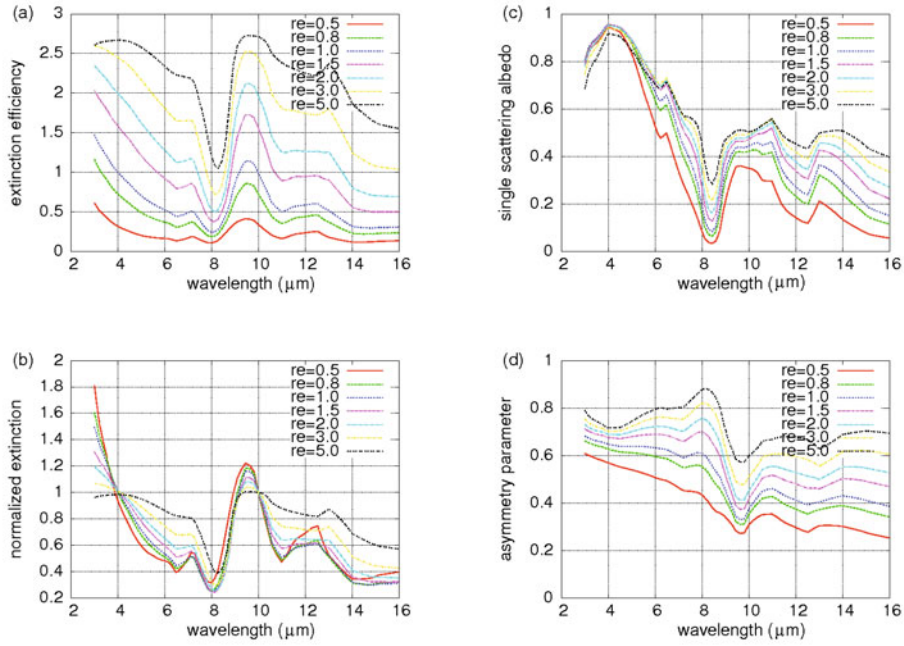

Figure 9.5 Effect of particle size distribution on dust optical properties. The extinction efficiency (a), the extinction normalized at 10 μm (b), the single scattering albedo (c) and the asymmetry parameter (d) are plotted from 3 to 16 μm for 7 effective radii "re", from 0.5 μm to 5.0 μm.

normalized extinction. Considering realistic effective radii for the coarse mode, between 1 and 3 μm, the spectral impact on extinction reaches 30% at its maximum. This agrees with Sokolik et al. (1998) simulations showing that, for many dust samples, the shape of extinction coefficient at infrared wavelengths remains almost unchanged when the mean dust radius increases. The impact on the single scattering albedo and the asymmetry parameter (which are less significant than extinction efficiency for longwave radiative transfer and aerosol retrievals) is of the same order of magnitude.

As we expect that readers are more familiar with aerosol remote sensing in the shortwave, we show on Figure 9.6 the variations of extinction from 0.5 to 15 μm for three effective radii. The situation differs greatly in the shortwave and in the longwave:

- from 3 to 15 μm, as mentioned previously, the three curves are very similar (the normalized extinctions are very close), which means that all the wavelengths are affected in the same way by a change in the particle size
- below 3 μm, the curves of extinction efficiency are not proportional but cross each other, which means that the relative sensitivity of wavelengths (or instrument bands) to the aerosol content is strongly dependent on particle size.

In short, the impact of PSD is crucial for aerosol remote sensing in the solar domain when using several channels, but it is less significant for the longwave domain. A final comment on Figure 9.6 is that the ratio between infrared and visible extinction (or AOD) increases with the effective radius, from 0.2 when re=1μm to 0.8 when re=3μm. This great variability explains why it is not possible to retrieve or extrapolate the infrared AOD from the visible AOD if the fine and coarse mode of the PSD are not perfectly known. This last comment implies that retrieval of infrared AOD from infrared observations is indispensable in order to estimate the aerosol forcing on the longwave radiation.

9.2.4 Effect of particle shape

With the exception of liquid aerosol particles as sulphate stratospheric aerosol that are obviously spherical, modeling the shape of aerosol particles is rather complex: observations show that dust exhibits a high variability of shapes (e.g. E.A. Reid et al., 2003 ; Chou et al., 2008). Until recently, this difficulty has led most authors to consider that dust particles were spherical when simulating their infrared optical properties.

However, over recent years, much laboratory work has been conducted to evaluate the effect of asphericity at infrared wavelengths (Hudson et al., 2007, 2008; Mogili et al., 2007 ; Kleiber et al., 2009). The comparison between laboratory measurements on elementary mineral aerosols tends to show that the Mie theory (i.e. the assumption of spherical homogeneous particles) fails to reproduce the extinction spectrum of minerals. Hudson et al. (2007) and Mogili et al. (2007) also showed that, surprisingly, simpler disc models (Bohren and Huffman, 1983) may work well in reproducing the position of the resonance band of clays or quartz which is shifted towards lower wavelengths when using the Mie theory. However, the results are less clear for the coarse mode particles where the Mie theory behaves better, and some uncertainty remains about the transposition of the laboratory work to the real atmospheric aerosol. As discussed in Kleiber et al. (2009), it is also possible that refractive indices directly measured in the collected atmospheric aerosol (and not on

individual minerals in bulk crystal samples) indirectly take into account the shape of the particle as this information could be incorporated in the refractive indices.

Amongst the available algorithms for computing optical properties for nonspherical aerosol particles, one of the most widely used is the T-matrix code by Mishchenko et al. (2002). The particles can be modeled as oblate or prolate spheroids (see Chapter 2), characterized by their aspect ratio. The aspect ratio of desert dust particles is usually in the [1.7–2.0] range (Mishchenko et al., 1997), as confirmed by numerous analyses of scanning electron microscope (SEM) images. However, shape observations by Nadeau (1987), for example, are consistent with the sheet-like mineral structure of silicate clays. Similarly, the best fits of measurement spectra with T-Matrix results assuming spheroid particles require highly eccentric oblate spheroids (for silicate clays) or a very broad distribution including both extreme oblate and prolate spheroids (Kleiber et al., 2009).

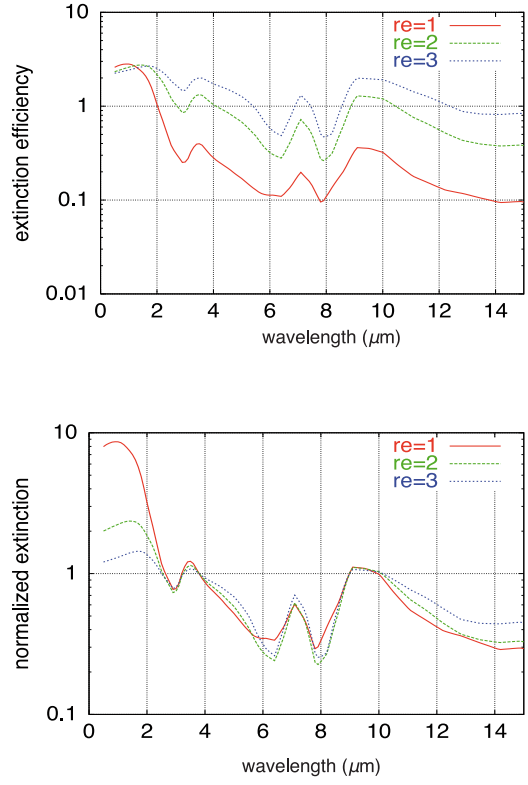

Figure 9.6 Effect of effective radius "re" on the extinction efficiency (top) and the extinction normalized at 10 μm (bottom) from 0.5 to 15 μm: comparison of the spectral behavior in the shortwave and longwave domains.

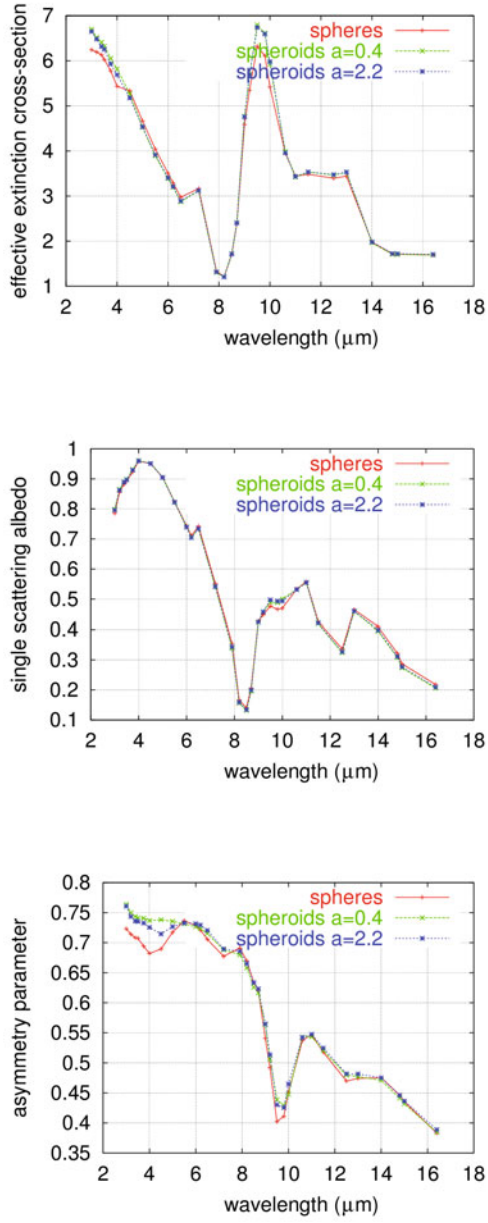

Figure 9.7 Effect of the aspect ratio of mineral dust particles on the optical properties from 3 to 16 μm.

Subsequently, the aim of the current paragraph is not a quantitative evaluation of optical properties for a realistic aerosol population but an estimation of the expected error when assuming spherical aerosol. We are thus only considering here an ensemble of randomly-oriented oblate or prolate spheroids with an aspect ratio varying from 0.4 to 2.2. This is quite an extreme range considering aspect ratios usually reported from SEM images. If we take a single value for the aspect ratio rather than a distribution, we might overestimate the impact of asphericity: Mishchenko et al. (1997) have shown that averaging over various aspect ratios tends to reduce the difference observed with spherical particles.

Simulations are performed using the T-matrix algorithm described in the book by Mishchenko et al. (2002) and available at http://www.giss.nasa.gov/staff/mmishchenko/t_matrix.html. The optical properties for three particle shapes, oblate spheroids (aspect ratio a=0.4), prolate spheroids (a=2.2) and spheres, are plotted on Figure 9.7. The differences between spheres and spheroids are minor: some discrepancy occurs around 4 and 9 μm only. The difference is maximal at precisely 3.75 and 9.5 μm. At these wavelengths, the optical properties C_{ext}, ϖ and g generally show a minimum for spheres and increase when the aspect ratio moves away from 1. The phase function for spheroids differs from the phase function for spheres only at 3.5 μm. By comparison, for shorter wavelengths (e.g. 0.55 μm), the sensitivity to shape is high for the phase function at high scattering angles (see Chapter 2). We must also underline here a difference between the longwave and the shortwave domains: the change in the phase function at high angles (120 to 180°) has very low impact on the satellite-based infrared observations. In fact, as the main source of the radiation, the Earth's surface, is "behind" the aerosol layer, the signature of aerosols from space in the longwave is primarily due to their extinction (while in the shortwave it is primarily due to the scattering of photons towards the instrument).

9.2.5 Summary

This section is summarized in Table 9.2 comparing the conclusions from this chapter with what occurs in the shortwave domain.

9.3 The radiative transfer equation in the thermal infrared range

Chapter 3 dealt with the radiative transfer equation in the shortwave domain, i.e. considering the sun as the only source of radiation. In this chapter, we establish the radiative transfer equation considering the Earth as the main source of radiation. The observed radiation is emitted by the Earth's surface and/or by the atmospheric layers. It is partly absorbed by the molecules and aerosols, and/or scattered by the aerosols: it thus contains the signature of the atmosphere.

First, let us introduce some specific vocabulary, avoiding equations.

The observation of the radiation in the infrared can be performed by a radiometer or by a spectrometer, located either on the ground, or onboard an aircraft, a balloon or a satellite.

Whereas a radiometer collects the photons to measure filtered radiance in a few wide spectral bands, a spectrometer measures the spectral radiance in many continuous, very narrow, spectral channels. A typical radiometer can have up to 20 spectral bands (or channels), whereas a typical spectrometer has several thousands channels (note that the word "band" is not used for spectrometers). The Atmospheric InfraRed Sounder AIRS (Aumann et al., 2003) or the Infrared Atmospheric Sounding Interferometer IASI (Chalon et al., 2001) are two examples of new-generation spectrometers.

Mineral aerosol microphysics	**Thermal infrared**	**Visible and solar infrared**
Refractive indices (composition)	+++ great impact -high spectral variability of indices (absorption peaks) -high inter-model variability - few bulk aerosol measurements - difficulty in handling the mixture of pure minerals (high geographical variability)	++ moderate impact - spectral dependency of indices relatively low and well-known - more observations
Size distribution	++ moderate impact - effect of the PSD width is extremely weak - coarse mode prevails - effect on normalized extinction, single scattering albedo and asymmetry parameter to the order of 30% at most - large impact on extinction efficiency if not normalized, but no effect for remote sensing applications	+++ great impact - relative sensitivity at different wavelengths depends on the PSD - accumulation and coarse mode must both be considered
Shape	+ (++?) *a priori* low impact - impact lower than 10% only around specific wavelengths for relatively moderate aspect ratios - laboratory measurements in progress tend to show that very eccentric aspect ratio should be considered	++ moderate impact - phase function at high angles is modified, which directly affects the observation from a satellite

Table 9.2 Influence of microphysical properties of dust aerosol on its optical properties and consequences for remote sensing applications. Comparison between shortwave and longwave domains.

The **spectral radiance** is the power received by the sensor facing a given direction, per surface unit of the receiver, per unit solid angle of its field of view, and per wavelength or wavenumber unit[2]. Thus, it can be expressed in W/(m^2.sr.μm) or W/(m^2.sr.cm^{-1}). However, it is often more convenient to consider an equivalent quantity: the **brightness temperature** (BT), in kelvin (K). The BT is defined as the temperature of a black body emitting the same spectral radiance at the same wavelength (by extension, at the central wavelength of the spectral channel being considered). Whereas the radiance varies by several orders of magnitude from the longer thermal infrared wavelengths to the shorter wavelengths, the brightness temperature scales the whole spectrum at comparable levels. Another reason why BT is convenient is that the brightness temperature measured from space is usually not far from the skin temperature of the surface (in atmospheric windows) or the thermodynamic temperature of the atmospheric level observed (in absorbing regions).

An important category of infrared radiometers or spectrometers on board satellites are **vertical sounders**, or just "sounders", which means that they provide information at several vertical levels in the atmosphere. Vertical sounders on board satellites have been used for decades to provide vertical profiles of temperature and water vapor for weather forecasting (McMillin et al., 1973). This ability to separate the radiation from several altitudes using the spectral information mostly relies on the absorption and emission by the molecules.

As it is critical for readers to figure out the "weighting function" of a spectral channel, indicating which slice of the atmosphere is preferentially observed, we will first try to define it on the basis of physical considerations, before introducing the formal equations in the next paragraph. We consider here an instrument on board a satellite observing the Earth downward.

Due to the **absorption** of the radiation by atmospheric gases (water vapor, ozone, carbon dioxide, etc.), the **transmission** of the upwelling radiation between an altitude level (or equivalently a pressure level) in the atmosphere and the satellite decreases when the altitude level decreases. For instance, if the transmission between the surface and the satellite is 0.5, only 50% of the radiation emitted by the surface can reach the satellite. The transmission between an elevated layer and the satellite is thus higher than 0.5 (e.g. the transmission could be 0.7 at 800 hPa). At the top of the atmosphere, which is usually fixed at a few pascals (between 50 to 100 km), the transmission reaches its maximum value of 1. Indeed, the radiation emitted by the top of the atmosphere in the direction of the satellite does not meet any absorbing molecule and reaches the satellite level without attenuation.

The **thermal emission** of an atmospheric layer (i.e. of the molecules and particles contained in this layer) is the physical mechanism counteracting the absorption; the higher the absorption of a medium, the higher its emission, following Kirchhoff's law. Out of two layers at the same temperature, the one that absorbs the most is also the one that emits the most. At the same time, considering two similarly absorbent layers at different temperatures, the warmer one will emit more radiation than the colder one.

2 For broad-band radiometers, the measured signal is sometimes given in term of integrated radiance, in W/(m^2.sr). The integrated radiance, which is instrument-dependent, is equal to the product of the spectral radiance with the instrument filter – or instrument spectral response function (ISRF) – integrated over the full range of observed wavelengths. See Section 9.3.1 and Eq. (9.17)

When absorption is strong enough, the surface and the lower part of the atmosphere might not be observed from space (then the total transmission is zero, see Figure 9.8, for example at 6 μm). On the other hand, the upper atmosphere cannot be observed either, because emission is negligible due to the scarcity of particles and molecules. This involves that only radiation emitted by a given intermediate range of vertical levels might be observed. It is the **weighting function** that gives the exact contribution of each atmospheric level to radiation going up to space. The weighting function usually shows a typical bell-shaped curve, see Figure 9.9 for a schematic illustration. As absorption depends on the wavelength, each spectral channel has its own weighting function (see Figure 9.10).

When absorption strength is moderate, the total transmission is no longer zero (see Figure 9.8, for example at 12 μm) and there is some contribution of the surface and lower part of atmosphere to the radiance outgoing to space. Then the weighting function curve is cut at the surface (see Figure 9.9).

Lastly, the special case with weak absorption corresponds to the so-called "window channels" (see Figure 9.8, for example at 4 μm) and a weighting function limited at the surface and quickly vanishing further up in the atmosphere.

Now that the reader is more familiar with the notions of sounding and weighting functions, let us build the radiative transfer equation (RTE) in the infrared, first without aerosols (Section 9.3.1) and then with non scattering and scattering aerosols (Sections 9.3.3 and 9.3.4). This is only a very short introduction to radiative transfer theory, and a far more detailed presentation can be found in the books from Liou (1980), Lenoble (1993) or Thomas and Stamnes (1999).

9.3.1 The RTE in an aerosol-free atmosphere

The hypotheses considered here are, for the sake of simplicity:

- a plane parallel atmospheric model;
- no refraction in the atmosphere;
- no sun (night observations only or wavelengths higher than 4 μm);
- no scattering (Rayleigh scattering by molecules is negligible in the longwave domain);
- local thermal equilibrium prevailing everywhere.

Modeling a spherical atmosphere or the refraction effects is not difficult, but beyond the scope of this book. The effect of sun radiation and scattering is introduced in Section 9.3.4. Firstly we develop a monochromatic case, i.e. considering a single wavelength, followed by the explanation of the convolution by the instrument spectral response.

Let us consider an infinitely small path in the atmosphere. The Beer-Lambert equation, already set out in this book (Chapter 2) introduces the extinction coefficient σ_{ext} as the proportion of energy lost per elementary length unit ds at a given wavelength

$$\frac{dI_\nu}{ds} = -\sigma_{ext}(\nu) I_\nu , \tag{9.1}$$

where I_ν is the spectral radiance at frequency ν.

Without scattering, the extinction is caused by absorption only and thus

$$\frac{dI_\nu}{ds} = -\sigma_{abs}(\nu) I_\nu . \tag{9.2}$$

However, the loss of energy by absorption is not the only process to consider. The atmospheric medium considered here also emits radiation, as any body at temperature T>0. Both processes, absorption and emission, are to be considered and thus the radiative transfer equation (RTE) in its differential form is

$$\frac{dI_\nu}{ds} = \sigma_{emis}(\nu) J_\nu - \sigma_{abs}(\nu) I_\nu , \tag{9.3}$$

where σ_{emis} is the emission coefficient of the body, and J_ν is the so-called source function.

In order to give the analytical expression of the source function, let us first introduce the concept of Local Thermodynamic Equilibrium (LTE). In the atmosphere, up to altitudes of roughly 60 to 70 km, the molecule density is such that the "thermal" emission (caused by collisions between molecules) is predominant and spontaneous emission of photons by molecules is negligible. In other words, the repartition of molecules in the energy levels is driven only by temperature: this is LTE. At higher altitudes where there is no LTE, the density of molecules is so low that this effect can be dismissed for a nadir sounder on board

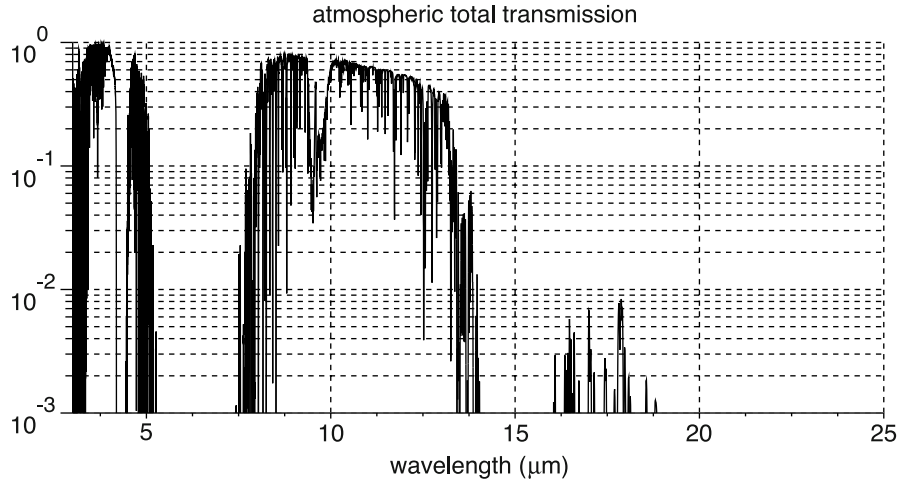

Figure 9.8 Total transmittance of the atmosphere from 3 to 25 μm, for a tropical situation without aerosol.

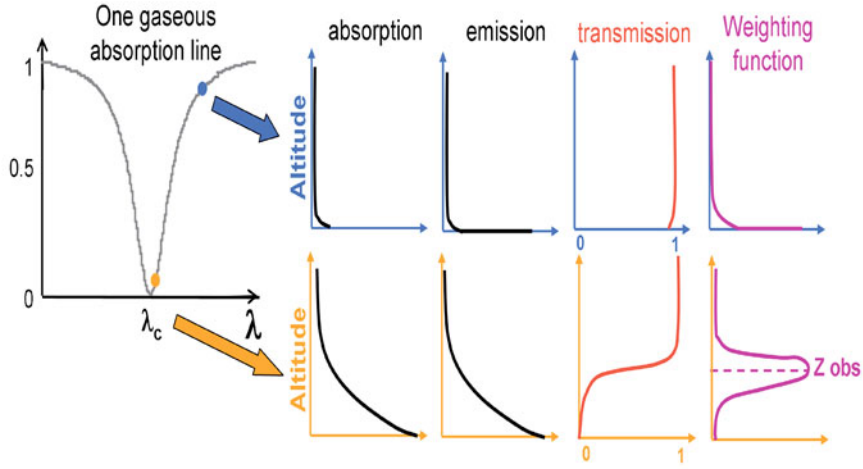

Figure 9.9 Simplistic view of the weighting function. If the gaseous absorption is low (blue dot), then, according to Kirchhoff's law, the emission is low and the atmospheric transmittance is almost equal to 1 down to the Earth's surface. The weighting function is zero except close to the surface (window channel). If the absorption is strong (orange dot), then transmission at the surface is zero and the weighting function peaks at an observation altitude Zobs (sounding channel).

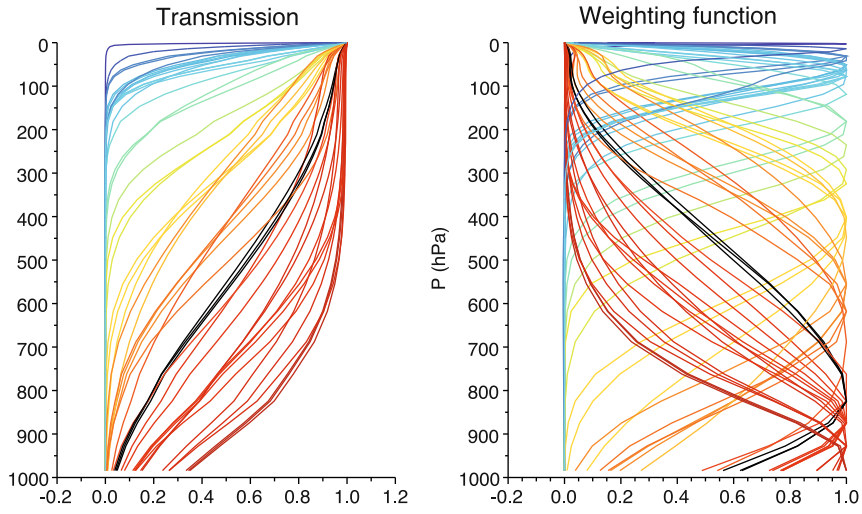

Figure 9.10 Examples of transmission profiles (left) and normalized weighting function (right) for the IASI instrument, for a subset of one over 10 channels in the spectral range [660–780] cm^{-1}. The color code indicates the altitude of the peak of the weighting function.

a satellite (looking down to the Earth's surface). Non-LTE must be taken into account for limb view sounders (looking to space through the atmosphere) (see Goody and Young's book, 1989), but this type of observation geometry prevents the observation of the lower atmosphere and is consequently out of the scope of tropospheric aerosol remote sensing.

Assuming LTE, the source function of each atmospheric layer depends on its temperature only and is given by Planck's law

$$J_\nu = B_\nu(T) = \frac{2h\nu^3}{c^2\left[\exp\left(\frac{h\nu}{kT}\right)-1\right]}. \tag{9.4}$$

This function, established by Max Planck in 1900, describes the spectral radiance of the radiation emitted at frequency ν by a blackbody at temperature T. It contains the following constants:

- c, velocity of light in the vacuum;
- h, Planck's constant;
- k, Bolzmann's constant.

Let us now introduce Kirchhoff's law of thermal radiation. The law states that, at thermal equilibrium, the emissivity of a body equals its absorptivity. Applying Kirchhoff's law locally in a given atmospheric layer gives the equality of absorption and emission coefficients

$$\sigma_{emis}(v) = \sigma_{abs}(v)$$

Thus, Eq. (9.3) can be written

$$\frac{dI_\nu}{dl} = \sigma_{abs}(\nu)\left(B_\nu(T) - I_\nu\right). \tag{9.5}$$

This equation is the differential RTE at local thermal equilibrium in a non-scattering medium. Another form of this equation may be preferred, using either the optical depth or the transmittance instead of the absorption coefficient.

The transmittance of a medium, between z and z' is defined as

$$t_\nu = \exp\left(-\int_z^{z'} \sigma_{abs}\, dl\right) = \exp(-\tau), \tag{9.6}$$

where we introduce τ, the optical depth of the layer between z and z'. This is equivalent to

$$\frac{dt}{t} = -\sigma_{abs}\, dl\,. \tag{9.7}$$

Using the above expression in Eq. (9.5), we obtain

$$\frac{dI_{\nu}(t)}{dt} = -\frac{1}{t}\left[I_{\nu}(t) - B_{\nu}(T(t))\right]. \tag{9.8}$$

We can also use the definition of the optical depth from Eq. (9.6) which results in

$$\frac{dI_{\nu}(\tau)}{d\tau} = -\left[I_{\nu}(\tau) - B_{\nu}(T(\tau))\right]. \tag{9.9}$$

For atmospheric studies, the radiative transfer equation is of more use in its integral form than in its differential form. So, we have to integrate the RTE between the Earth's surface and the satellite. We first consider a nadir view (i.e. the angle between the local vertical at the Earth's surface oriented downward and the satellite viewing direction is 0°). The integrating path is along the vertical axis, going from 0 (at the surface) to the top of the atmosphere.

The integration gives the spectral radiance at the top of the atmosphere, assuming a surface emissivity of ε_{surf} (between 0 and 1)

$$I_{\nu} = \varepsilon_{surf} B_{\nu}(T_{surf}) \exp(-\tau_{surf}) + \int_0^{\tau} B_{\nu}(T(\tau)) \exp(-\tau) d\tau + (1 - \varepsilon_{surf}) \exp(-\tau_{surf}) \int_{\tau}^{0} B_{\nu}(T(\tau)) \exp(-\tau) d\tau. \tag{9.10}$$

Three terms appear in Eq. (9.10): the first is the radiation emitted by the surface and transmitted to the satellite; the second is the so-called "upward" radiation emitted by the atmospheric layers; the third is the "downward" radiation emitted by the atmosphere and reflected by the surface. Obviously, the sum of the surface reflection coefficient and emissivity equals 1. Note that the surface emissivity is sometimes close to 1 (e.g. 0.99 over the ocean, around 10 μm), so the third term can be disregarded in the RTE in these cases.

The same equation as a function of transmittance t is

$$I_{\nu} = \varepsilon_{surf} B_{\nu}(T_{surf}) t_{surf} + \int_0^1 B_{\nu}(T(\tau)) dt + (1 - \varepsilon_{surf}) t_{surf} \int_1^0 B_{\nu}(T(\tau)) dt \,, \tag{9.11}$$

and, after replacing the integration variable *dt* by *d(ln(P))* with *P* the pressure at a vertical level, it becomes

$$I_\nu = \varepsilon_{surf} B_\nu\left(T_{surf}\right) t_{surf} + \int_{\ln(Psurf)}^{-\infty} B_\nu\left(T(P)\right) \frac{\partial t(P)}{\partial \ln(P)} d\ln(P) + \left(1-\varepsilon_{surf}\right) t_{surf} \int_{-\infty}^{\ln(Psurf)} B_\nu\left(T(P)\right) \frac{\partial t(P)}{\partial \ln(P)} d\ln(P). \tag{9.12}$$

This provides the opportunity to introduce the weighting function

$$W(P) = \frac{\partial t(P)}{\partial \ln(P)} . \tag{9.13}$$

The weighting function is thus defined as the derivative of the transmission with respect to the pressure logarithm (or altitude). Its name comes from its role in the RTE: if we consider, for example, the upward term, the radiation emitted by each layer *B(T(P))* is weighted by the weighting function *W*. The maximum contribution comes from the pressure levels where *W* is maximum, which corresponds to an inflection point on the transmission profile. A sketch of the weighting function is given in Figure 9.10.

When the local zenith angle θ (angle at the ground surface between the local vertical and the satellite direction) is not equal to 0, then we introduce the secant of this angle, using $\mu = cos(\theta)$

$$\sec(\theta) = \frac{1}{\mu} , \tag{9.14}$$

and Eq. (9.5) becomes

$$\mu \frac{dI_\nu}{dl} = \sigma_{abs}(\nu)\left(B_\nu(T) - I_\nu\right), \tag{9.15}$$

and the transmission becomes

$$t_\nu = \exp\left(-\int_z^{z'} \frac{1}{\mu} \sigma_{abs} dl\right); \tag{9.16}$$

so that Eq. (9.13) is unchanged (this is an advantage of working with transmission rather than optical depth).

Readers will have noticed that the previous equations are all monochromatic. Indeed, in the infrared domain, the gaseous absorption lines are so numerous and thin that an accurate simulation requires a line-by-line approach. A real instrument never senses a single wavelength but over a wavelength range constituting a channel, the radiative contribution of each wavelength being weighted by the so-called instrument spectral response function (ISRF), or instrument line shape (ILS), or sometimes also referred to as the convolution function. Thus, the last step of the simulation of the radiative transfer usually consists in the

convolution by the ISRF f_i of each channel i through the normalization

$$I_i = \frac{\int f_i(\nu) I(\nu) d\nu}{\int f_i(\nu) d\nu}. \tag{9.17}$$

9.3.2 The data required as input for a gaseous atmosphere

A short analysis of the integrated RTE gives us the main variables to take into account.

The first one is the temperature, not only of the surface (skin temperature), but also at every level in the atmosphere. Indeed, the radiation emitted by the surface and by each atmospheric layer is directly dependent on the temperature through Planck's function. A second surface parameter of importance is the emissivity (related to the materials at the surface). The surface pressure (related to the altitude and the meteorological situation) also needs to be taken into account.

A third variable is the transmittance profile, which is equivalent to the absorption or optical depth profiles. The absorption of photons is caused by rotation and vibration transitions of atmospheric gas molecules. In a given layer of pressure P, the total optical depth of absorption is the sum of the optical depths for all species with absorption lines at the given wavelength

$$\tau(P,\nu) = \sum_j \tau_j(P,\nu). \tag{9.18}$$

The optical depth for an individual gas at a given wavelength is the product of its absorption efficiency (for a single molecule) by the number of molecules

$$\tau(P,\nu) = \sum_j \sigma_{abs\,j}(P,T(P),\nu) N_j(P). \tag{9.19}$$

The absorption efficiency of a molecule depends on the frequency, but also on the thermodynamic conditions (mainly the temperature and pressure). Indeed, absorption lines corresponding to transitions between two states of energy, their intensity, width and shape depend on partial pressure of the gas in question and other gases, and the temperature. The spectral width of a line, for example, is due to collisions between molecules (which obviously depend on pressure) and to the Doppler effect. However, the accurate description of these spectroscopic effects and line modeling is beyond the scope of this book, and can be found in Bernath (2005).

Consequently, the concentration profile ($N_j(P)$) must be known for each gas that has a non-negligible absorption. Also, gaseous spectroscopy (for water vapor, ozone, carbon dioxide…) is a necessary input. All the parameters needed to compute absorption line shape and intensity can be found in the GEISA (Jacquinet-Husson et al., 2008) or HITRAN (Rothman et al., 2009) spectroscopic databases, both available on the Internet: http://ether.ipsl.jussieu.fr/ (GEISA) and http://www.cfa.harvard.edu/hitran/ (HITRAN). These data-

bases compile results from the work of teams at many spectroscopic laboratories. For instance, the GEISA-09 sub-database of line transition parameters involves 50 molecules (111 isotopic species) and contains 3,807,997 entries.

All the variable parameters (thermodynamic profile, i.e. temperature and humidity profiles, other gas concentration profiles and Earth's surface temperature, emissivity and pressure) must be known with sufficient accuracy for remote sensing applications.

The surface temperature and the surface emissivity over land might come from the instrument observations themselves (Péquignot et al., 2008, Chédin et al., 2004). The surface emissivity might also come from a climatological data set (e.g. the ASTER spectral library, available at http://speclib.jpl.nasa.gov/), thus offering the possibility to easily retrieve the surface temperature from a window channel. However, the surface emissivity can be highly variable in space (low emissivity over deserts or bare soils, high emissivity over forest or ocean) and in time (seasonal cycle related to the growth of vegetation). This difficulty explains why retrieval algorithms in the infrared are usually first developed over oceans, where the emissivity is well known, almost spatially homogeneous and almost spectrally constant (close to 1 in the thermal infrared). The surface pressure is usually known with sufficient accuracy by just considering the altitude of the ground pixel.

The temperature and humidity profiles can be obtained from in-situ radiosoundings, Numerical Weather Prediction (NWP) models, or sounder retrievals. However, when using sounder retrievals for aerosol remote sensing applications, great care must be taken not to choose channels sensitive to aerosols when retrieving the thermodynamic profile. Not only the profile of water vapor but also the profile of other gases must be provided: ozone, for instance has strong absorption lines between 9 and 10 μm, in the middle of the window 8–12 μm which is of particular interest for aerosols. Other gases absorbing in the infrared range are CO_2, CH_4, CO, etc. If the gas variability with time and space is low, or if the channel chosen has a weak sensitivity, then a constant profile can be assumed (for instance, for CO_2). Otherwise, highly variable gas absorption lines are usually avoided for aerosol remote sensing applications. Water vapor strong lines are to be avoided as much as possible. However, theses lines are so numerous, and there is a continuum of water vapor absorption, so the impact of water vapor can not be dismissed. Henceforth, we shall refer to the vertical profiles of temperature and all the absorbing gases (essentially water vapor) in the spectral domain of interest as the "atmospheric situation".

We should also mention climatologic databases containing a huge sample of atmospheric situations (e.g. the Thermodynamic Initial Guess Retrieval – TIGR- database from Chédin et al. (1985), and Chevallier et al. (1998)) that can be used for sensitivity studies or for the look-up tables approach of aerosol remote sensing.

We illustrate in Figure 9.11 the sensitivity of the radiative transfer to atmospheric and surface parameters with some typical examples of infrared spectra (without scattering).

9.3.3 The particular case of RTE in an atmosphere containing non-scattering aerosol

When the scattering of the particles can be neglected, the RTE for a gaseous atmosphere remains valid, with the addition of aerosol absorption optical depth to molecular optical depths. The transmittance is now the product of particles and molecules transmittances

$$t_\nu = \exp\left(-\int_z^{z'}\left(\sigma_{molecules} + \sigma_{particles}\right)dl\right) = t_\nu^{molecules}\, t_\nu^{particles}. \tag{9.20}$$

The transmission from the Earth's surface to the satellite must also be modified in the same manner. This particular case applies mainly for stratospheric volcanic aerosols due to their refractive indices.

Although very simple, this formulation of the RTE is quite useful as it gives us the contribution of aerosol absorption and emission to the radiance. If the single scattering albedo is not too high, the main effect of aerosols on the brightness temperature spectrum is a cooling effect.

Indeed, the total transmittance decreases, and the Earth's surface contribution (first term in Eq. (9.10), which is the dominating term for channels of interest to aerosol remote sensing, decreases as well. The second term in Eq. (9.10), of atmospheric contribution, is also

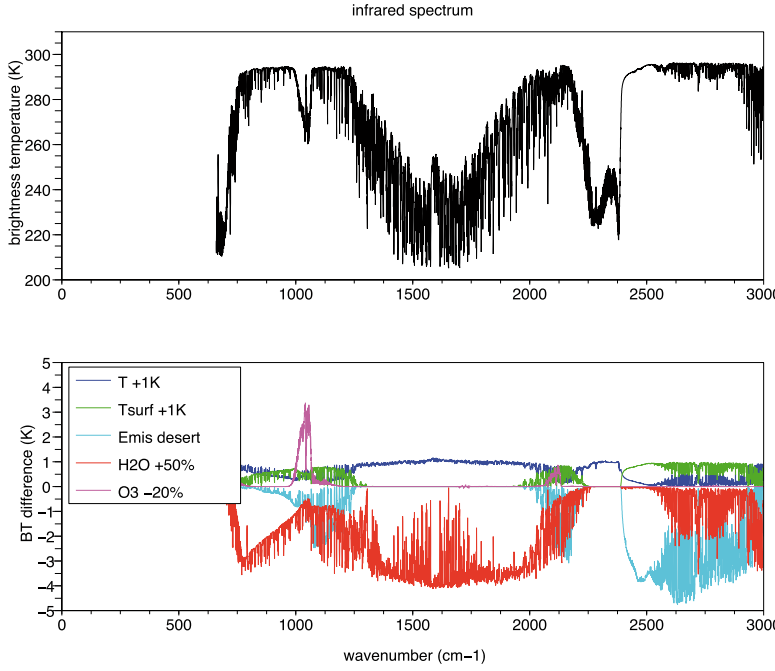

Figure 9.11 Top: infrared spectrum convolved with the IASI instrument response function, in brightness temperature (night-time, over ocean, no aerosol); bottom: the infrared spectrum sensitivity to a change in the atmosphere or the surface (blue: temperature profile, green: surface temperature, cyan: surface emissivity, red: water vapor, pink: ozone profile).

modified: the transmittance at levels inside the aerosol layer and below, is lower. Thus, the weighting function is increased at all the levels where aerosol is present. This means that the relative contribution of the black-body radiation emitted at these levels to the total observed radiance increases. If the aerosol is located at altitudes where the temperature is lower than the mean BT seen by the channel, which is usually the case for channels peaking close to the surface, then the second term in Eq. (9.10) also gives a decrease of the BT in presence of absorbing aerosols.

9.3.4 The RTE with scattering processes

As previously shown (considering the values of single scattering albedo of Figure 9.3), scattering cannot be ignored in the presence of aerosols such as desert dust. Thus, the RTE must be modified by introducing scattering.

Let us assume that the electromagnetic wave propagates in the direction (θ,ϕ) and let $\mu=\cos(\theta)$. In a scattering medium of single scattering albedo ϖ and phase function p, the differential form of the RTE in Eq. (9.8) becomes

$$\frac{dI_\nu(t,\mu,\varphi)}{dt} = -\frac{1}{t}I_\nu(t,\mu,\varphi)+\frac{1-\varpi}{t}B_\nu(T(t))+\frac{\varpi}{(4\pi)t}\int_0^{2\pi}\int_{-1}^{1}p(t;\mu,\varphi;\mu',\varphi')I(t,\mu',\varphi)d\mu' d\varphi'. \tag{9.21}$$

The Planck emission of the medium which is no longer a black body is reduced by the scattering (second term), but the scattering itself contributes to the radiation in the direction (μ,ϕ), depending on the phase function (third term in Eq. (9.21).

If solar radiation from direction (θ_s,ϕ_s) cannot be dismissed (e.g. for shorter wavelength up to 4 μm during daytime), then a fourth term must be added to the previous equation

$$J_{sun}=\frac{\varpi}{(4\pi)t}I_{sun}p(t;\mu,\varphi;\mu_S,\varphi_S)t^{\mu/\mu_S}, \tag{9.22}$$

where I_{sun} is the solar radiance at the top of the atmosphere and $\mu_s=1/\cos(\theta_s)$ is negative.

The RTE is now an integro-differential equation with no analytical solution. Several numerical techniques have been developed to solve this problem, for example the Discrete Ordinate algorithm (DISORT), the method of the successive orders of scattering, or the two-stream approximation (see Chapter 2 or below). For a detailed description of these techniques, readers may refer to the books from Thomas and Stamnes (1999) or Hanel et al. (2003).

In some cases, a simplification might occur. Let us separate the radiance I into I+ and I-, with I+ the upwelling radiance and I- the downwelling radiance. These radiances and the phase function might be decomposed in Fourier series over ϕ-ϕ_0 where ϕ_0 is the azimuthal solar angle

$$I_\nu^{\pm}(t,\mu,\varphi)=\sum_{i=0}^{m}I_{\nu,m}^{\pm}(t,\mu)\cos(m(\varphi-\varphi_0)). \tag{9.23}$$

When applying the RTE to the m[th] Fourier component, we obtain a more useful form for numerical integration

$$\frac{dI^{\pm}_{\nu,m}(t,\mu)}{dt} =$$
$$-\frac{1}{t}I^{\pm}_{\nu,m}(t,\mu)+\frac{1-\varpi}{t}B_{\nu}(T(t))+\frac{\varpi}{(4\pi)t}\int_{-1}^{1}p_m(t;\mu;\mu')I^{\pm}_{\nu,m}(t,\mu)d\mu'+\frac{\varpi}{(4\pi)t}I_{sun}p_m(t;\mu;\mu_0)I^{\pm}_{\nu,m}(t,\mu). \quad (9.24)$$

Further simplification can arise, for instance if the solar radiation can be ignored. Figure 9.12 shows that the effect of solar radiation might be ignored, either by night or for wavelengths higher than 4.2 μm for a satellite instrument viewing at the Earth's surface. In that case, if the phase function has a revolution symmetry, which is what is usually observed for aerosols, then the azimuthal dependency is removed and only for m=0 is the Fourier component not null.

9.3.5 Solving the RTE

A numerical solution of the RTE equation can be computed with a code coupling a line-by-line model (required by the very thin spectral lines of molecules and the very high spectral resolution of infrared sounders) and a scattering algorithm, such as DISORT (Discrete ordinate algorithm, first described by Chandrasekar (1960)) or SOS (successive orders of scattering) algorithm (e.g. Hansen and Travis, 1974; Heilliette et al., 2004) or the adding-doubling algorithm (Van de Hulst, 1963; Liou, 2002). The DISORT algorithm has been coded by Stamnes et al. (1988) and is available as a Fortran subroutine.

In a coupled code (for example Dubuisson et al. (1996) or the 4A/OP code originally from Scott and Chédin (1981), and described in Chaumat et al. (2009)(see also http://ara.lmd.polytechnique.fr), the input requires the usual parameters of the line-by-line absorption code as described in Section 9.3.2, and additional parameters needed for the simulation of scattering. The DISORT or SOS scattering codes require the gaseous optical depth profile (that is, an output of the line-by-line absorption code) and aerosol parameters. The scattering parameter (extinction, single scattering albedo and phase function) are needed at each vertical level, but we usually assume that only the aerosol content varies with altitude. Note also that the Henyey-Greenstein approximation is often used instead of the full phase function. The Henyey-Greenstein approximation consists of replacing the phase function by a function of the asymmetry parameter g only. The approximated phase function defined from g differs from the true one at high scattering angles (i.e. for backscattering), but this has a negligible impact on the infrared radiance.

Such a coupled code is very accurate and is needed as a reference code. However, in the line-by-line case, computation is still time-consuming, so various techniques have been suggested to speed up the calculation, by taking into account the instrument spectral response function: k-distribution (e.g. S. Yang et al., 2000 ; Lacis and Oinas, 1991), spectral averaging (e.g. in the 4A/OP code).

Two situations in particular can benefit from faster algorithms. First, for window channels and dry atmospheres, when there is no (or almost no) gaseous absorption, the radiative transfer equation can be written much more simply, and can be solved, for instance, with the two-stream algorithm (Meador and Weaver, 1980). Second, for broad-band channels, band models, which are much faster than line-by-line models, can be used, for example the MODTRAN code (Berk et al., 1989) or Streamer (Key and Schweiger, 1988).

9.3.6 Aerosol effect on the longwave spectrum

The main difficulty for aerosol remote sensing in the longwave is that the sensitivity of brightness temperature (BT) to atmospheric temperature, water vapor and surface state is very high, and the aerosol has only a second-order impact, as illustrated in Figure 9.13. Indeed, a change from a typical tropical atmosphere to a mid-latitude atmosphere decreases the BT by several tens of kelvins, whereas the effect of the aerosol is usually in the range of a few kelvins.

A second difficulty is that the impact of aerosols on the observed radiance is also strongly dependent on the underlying atmospheric situation. For example, an aerosol of fixed optical depth, single scattering albedo and phase function profile might decrease the brightness

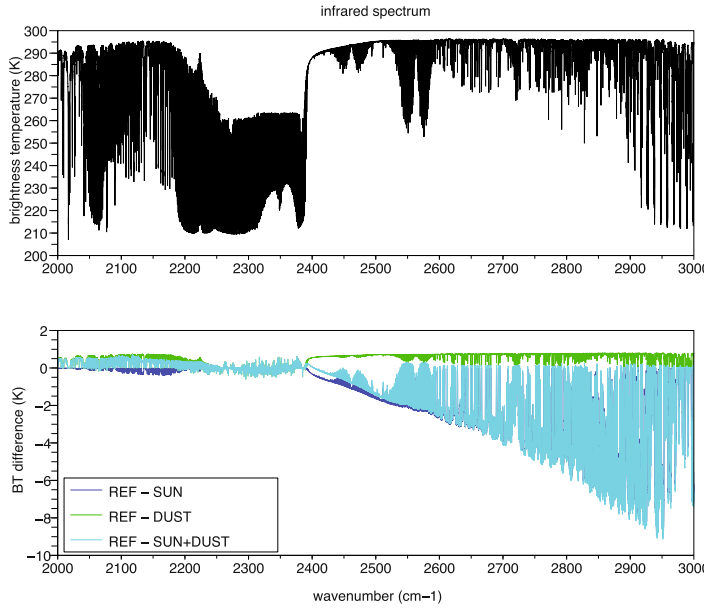

Figure 9.12 Top: simulated infrared spectrum in the medium infrared domain (2000 to 3000 cm^{-1}); the effect of solar radiation must be taken into account in this spectral domain; bottom plot: difference in BT (K) between the reference spectrum (no sun, no aerosol), and the same situation with sun only (blue), dust only (green) or sun and dust (cyan).

temperature by 6 K for a given atmospheric situation, and by only 2 K for another one with a different temperature and water vapor content, all other things being equal. As shown in Figure 9.14, this variability is observed both for window channels (AIRS channel #315 has a surface transmission greater than 0.9), mainly caused by a change in surface temperature, and for sounding channels (AIRS channel #134 has a surface transmission of about 0.55).

To sum up:

- The absolute value of BT depends on the surface and atmospheric thermodynamic situation.
- The relative effect of the aerosol on BT strongly depends on the surface and atmospheric thermodynamic situation.

We focus now on the effect of optical properties (single scattering albedo, asymmetry parameter, AOD) on the observed brightness temperature. Observing simulation results by night in Figure 9.15, it can be noted that:

- The effect of the single scattering albedo is complex: in this example, the sign of the albedo impact can be either positive (e.g. channel at 3.82 μm) or negative (e.g. channel at 11.48 μm) depending on the wavelength. This can be explained by a trade-off between two effects: in the RTE with scattering Eq. (9.21), the emitted radiation (second term), is weighted by (1-ϖ), whereas the scattered radiation (third term) is weighted by ϖ.

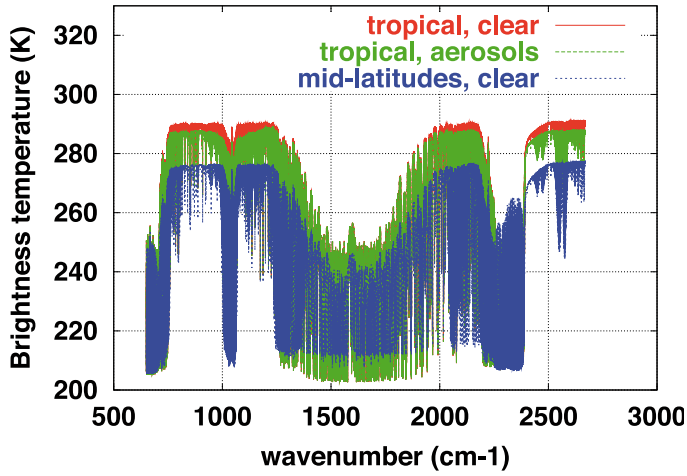

Figure 9.13 Comparison between the latitudinal effect (humidity and temperature profile) and the aerosol effect (Mineral Transported model from OPAC data-base) on the longwave spectrum: simulations for night-time, over oceans.

- The BT increases with the asymmetry parameter g: if g is close to 1, then forward scattering (in the direction of the satellite) is favored, while radiation lost by scattering is reduced (no solar radiation is assumed here).
- The BT decreases when the AOD increases, all other parameters being unchanged. This can be easily understood if the aerosol emission is lower than its extinction, which is generally the case for a temperature profile decreasing with altitude: when the aerosol extinction increases, the number of photons emitted by the surface and the atmosphere and reaching the satellite decreases.

These results are obtained for a single thermodynamic atmospheric situation (i.e. a single temperature and humidity profile). However, some cases might occur where the behavior changes. For instance, in case of very strong temperature inversion in the lower layers (a situation sometimes occurring by night), the emission from the aerosols might then prevail over the absorption and thus the BT might increase with AOD. Also, if the weighting function of the channel peaks higher in the atmosphere (strong absorption by gases), then the relative impact of the aerosol would change, but it would remain very low in the absolute, which is not a useful configuration for aerosol remote sensing.

These simulations show that the radiative effect of atmospheric aerosol on atmospheric spectrum is difficult to predict without a proper radiative transfer model, when both scattering and absorption occur. However, BT varies smoothly with optical properties, thus enabling some linear interpolations in order to avoid long computations.

We now focus on a specificity of infrared observation: the role of vertical distribution of aerosols on the observed signal. Not only can the quantity of aerosol at each level (i.e. the AOD within each atmospheric layer) change, but the single scattering albedo and asymmetry parameter can also vary, for instance if the size distribution or the composition of particles is modulated with the altitude. However, as there are very few experimental data of such variations, we are restricting these considerations here to the effect of the extinction vertical profile, assuming albedo and phase function constant over the whole atmospheric column.

We deal firstly with tropospheric aerosols, such as dust, located in one single atmospheric layer of the model. Note that radiative transfer codes usually work with the pressure as a vertical coordinate (and not the altitude). However, it is rather simple to convert a pressure grid to an altitude vertical grid (if a moderate accuracy can be accepted) and so we will generally present results using the vertical altitude. Figure 9.15 gives the sensitivity of BT to the layer altitude at two wavelengths (3.82 μm and 11.48 μm). The higher the layer, the greater its impact on the BT. Indeed, in the troposphere, the higher the aerosol layer, the lower its temperature, which reinforces the aerosol signature through the contrast between the radiation emitted by the surface and the radiation emitted by the aerosol. Secondly, when the aerosol is close to the surface, the absorption of radiation by gases between the aerosol layer and the satellite partly (or totally) hides the aerosol signature. This is why a change of altitude of the aerosol layer does not have a major impact on a window channel (at 3.82 μm here, the surface transmittance is greater than 0.9, whereas at 11.48 μm it is only 0.25). So, not only is there an impact from aerosol altitude on the signal observed, but also this impact depends on the wavelength (through the effect of gas absorption). Another

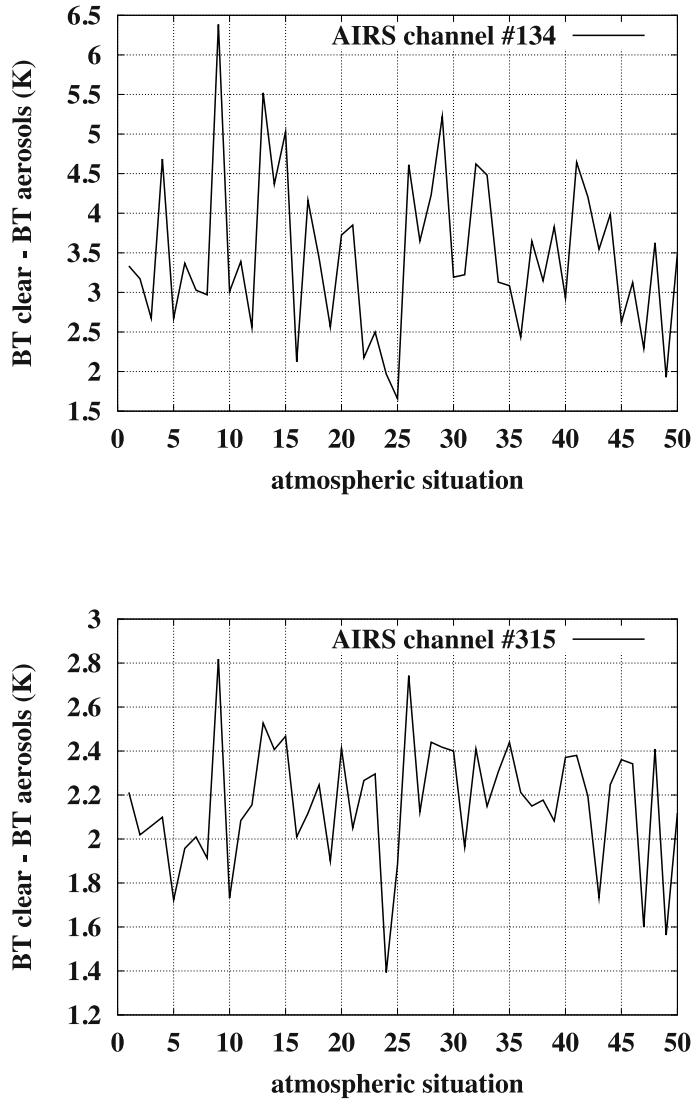

Figure 9.14 Examples of calculated impact of an aerosol layer on the brightness temperature measured by 2 AIRS channels: channel #134 at 843 cm^{-1} (top) and channel #315 at 2616 cm^{-1} (bottom). Nighttime simulations over oceans. The impact strongly depends on the thermodynamic atmospheric situation (i.e. T, H_2O and O_3 vertical profiles, taken in the TIGR database).

way to analyze this effect is to consider the aerosol layer temperature: as the temperature decrease in the troposphere is nearly uniform, the information about aerosol plume altitude or the information about its temperature are roughly equivalent. These considerations make aerosol remote sensing rather difficult in the longwave domain, but they do provide the unique possibility of measuring their altitude from space (using passive remote sensing).

In the case of aerosol profiles with complex structures (for example, two overlapping layers), it can be shown that the altitude retrieved corresponds to the median altitude in terms of infrared extinction. In other words, half of the AOD comes from aerosol below the retrieved altitude, and half comes from above. Except for perfect window channels with a transmittance of 1 (which do not really exist…), there is a particular case where the altitude can be disregarded: stratospheric aerosols observed with channels sounding the low troposphere. Indeed, for these low peaking channels, the transmittance at aerosol altitude is close to 1 and the pressure dependency in the RTE is removed.

Conversely, the infrared radiation is not as sensitive to the particle size or shape (all other things being equal, especially the infrared AOD at 10 μm), as can be seen on Figures 9.16 and 9.17. Of course, if the shortwave AOD, or the number density or mass density was kept constant, the size effect would be larger. This is why it is appropriate to retrieve the aerosol infrared optical depth from longwave observations. Figures 9.16 and 9.17 correspond to simulations performed with a relatively high amount of dust, with the AOD at 10 μm being 0.6. Thus, we conclude that the effect of size (less than a kelvin) and shape (a few tenths of a kelvin), can be dismissed on a first approach. This also means that the retrieval of size or shape requires firstly that the aerosol infrared AOD and altitude be well known.

9.4 Inversion principles

The previous paragraph described the direct problem: the modeling of the aerosol effect on measurements. We now focus on the inverse problem: the retrieval of some aerosol properties from observations. Even though there might be many more spectral measurements than unknowns (in the case of high resolution spectrometers), this inverse problem is ill-posed, as only one or a few quantities of interest to aerosols can be retrieved, and not the full description of the vertical profile of all the optical or microphysical properties of the aerosol. So, a careful sensitivity study, using radiative transfer simulations, can select the observable parameters and is a prerequisite to any inversion algorithm design. Indeed, an ill-posed problem can be solved only by introducing *a priori* knowledge, for example using parameterization (i.e. reduction of the number of unknowns through the description of the aerosol by a limited number of parameters) or using regularization (*a priori* of smoothness, for instance).

We have seen that many geophysical parameters not related to the aerosol, like the surface or atmospheric temperature, influence the radiative transfer. Therefore, these parameters must be either known *a priori* (from NWP analysis, or from another instrument), or retrieved (in a first-step process or simultaneously with the aerosol inversion), or by-passed by determining a combination of channels removing their influence.

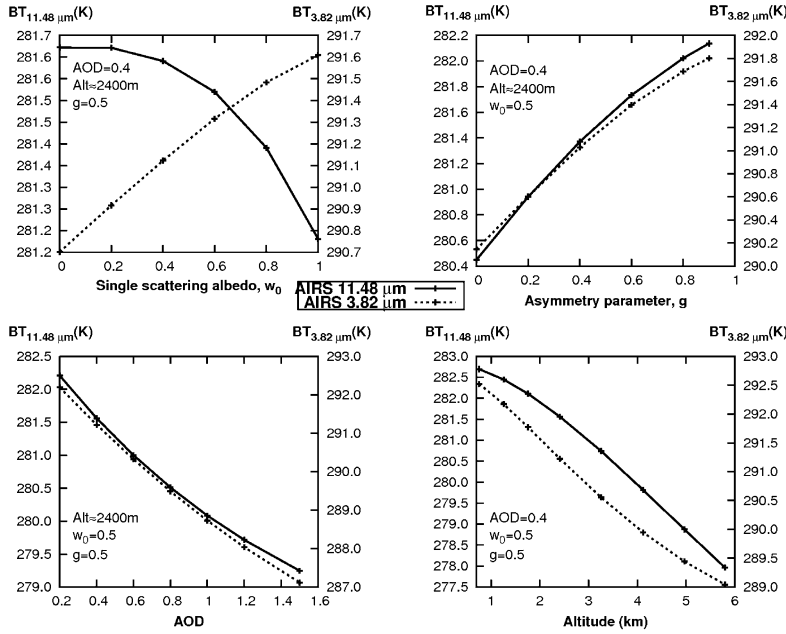

Figure 9.15 Simulated effect of aerosol optical properties and altitude on brightness temperature for 2 AIRS channels corresponding to the wavelengths 11.48 μm (thick line) and 3.82 μm (dotted line).

The purpose of this paragraph is to describe the great diversity of retrieval algorithms that can be used in the longwave domain for aerosol remote sensing. However, readers must bear in mind that the algorithm strongly depends on the instrumental data type (broadband radiometer or spectrometer, on ground or on board a satellite) but also on the purpose of the retrieval. For instance, an aerosol retrieval designed for near real-time monitoring in the framework of air quality must be fast enough. For a regional case study, some parameters in the algorithm might be tuned "by hand", whereas global retrievals for climate studies must be resistant to any local change.

9.4.1 Useful spectral domain

In order to have an impact on the observed radiance, the transmission from the aerosol layer to the satellite must be sufficiently high. This is why most channels are selected within, or close to, the atmospheric windows: around 4 μm, 8 μm and 10.5–12 μm. The water vapor absorption lines in fact totally preclude the use of the 5–8 μm band, not only because of the low transmission but also because the water vapor variability is extremely

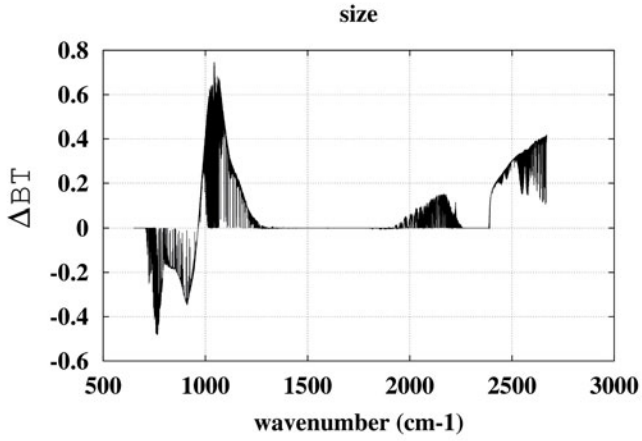

Figure 9.16 Simulated effect of the effective radius on the infrared spectrum: difference in brightness temperature between a spectrum computed with an effective radius of 3 μm and a radius of 1 μm. Night-time simulation over ocean, for a high mineral dust load.

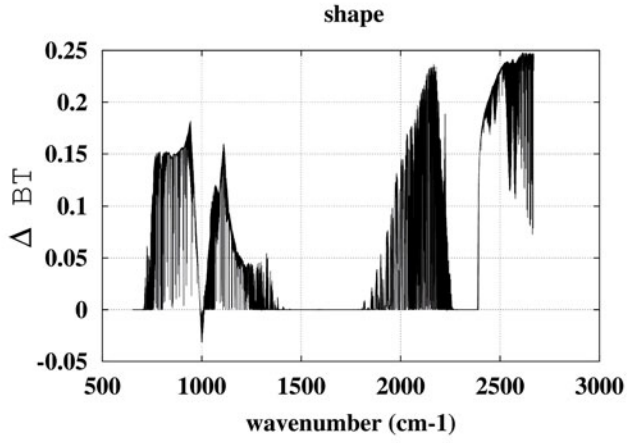

Figure 9.17 Simulated effect of the particle shape on the infrared spectrum: difference in brightness temperature between a spectrum computed with a spheroid – aspect ratio of 2 – and a sphere. Night-time simulation over ocean, for a high mineral dust load.

high. To a lesser extent, the same reason holds for the ozone band centered at 9.6 μm, which must be avoided.

The 8–12 μm band is appropriate for dust (which has a strong absorption band around 9 μm, see Section 9.2.2) but also for volcanic ash or volcanic sulphuric acid droplets.

Combining observations from the medium infrared band (3–4 μm) and the thermal infrared band (8–12 μm) is useful to discriminate the aerosol AOD from its height (or equivalently the aerosol layer temperature), as the respective sensitivities differ: Figure 9.18 shows that the sensitivity to a change in the aerosol altitude is stronger in the thermal infrared domain than in the medium infrared domain.

For recent infrared sounders, a channel selection is usually first needed to limit the computation time, because of the very high number of spectral channels. The number of channels to be used depends on the computation time and the number of observations to be retrieved, and can vary from 2 or 3 for global processing of measurements over long periods to over 100 for case studies (e.g. Carn et al., 2002). The channel selection for aerosol retrieval generally relies on statistics obtained from a high number of radiative transfer simulated spectra or Jacobians (the partial derivatives of the radiance with respect to a change in the aerosol optical depth or altitude). Sensitivity to aerosol must be as high as possible, together with a sensitivity as low as possible to variable gas (water vapor and ozone mainly, but also carbon monoxide or methane). The channels which are less affected by the aerosol (for instance at a wavelength where the aerosol extinction efficiency is relatively low) but which have similar weighting functions are also useful to constrain the emission from Earth's surface and atmosphere. Selecting channels with different transmissions of the gaseous atmosphere brings vertical information too: a proper coverage of the lower tropospheric column is ensured by selecting channels with transmittance varying in the range [0,1], because the lower the transmittance, the higher the altitude of the channel weighting function peak (see Section 9.3).

9.4.2 Preliminary steps

Building an aerosol-dedicated cloud mask

Distinguishing aerosols from clouds is always a tricky problem for aerosol remote sensing (King et al., 1998). Henceforth, we shall refer to a scene without aerosols or clouds as "clear" or "aerosol-free", and a scene with a water or ice cloud as "cloudy" and a scene with aerosol particles as "aerosol". Note that the cloudy scenes might also contain aerosols but are disregarded anyway, even if Hong et al. (2006) have shown that it should be possible to distinguish co-existing cirrus-dust scenes from those associated only with cirrus clouds or dust alone.

Usually an aerosol-dedicated cloud mask must be developed, because standard cloud masks used for meteorological applications need a high confidence in clear sky detection and are consequently designed to filter both water/ice clouds and aerosols together (e.g. EUMETSAT, 2009). Very thick clouds are usually easy to detect (they correspond to very cold BT) and the principal difficulty lies in the detection of thin cirrus clouds and low altitude clouds. The accurate description of clouds' edges might be another concern for imaging instrument with high spatial resolution. The detection by daytime of low altitude

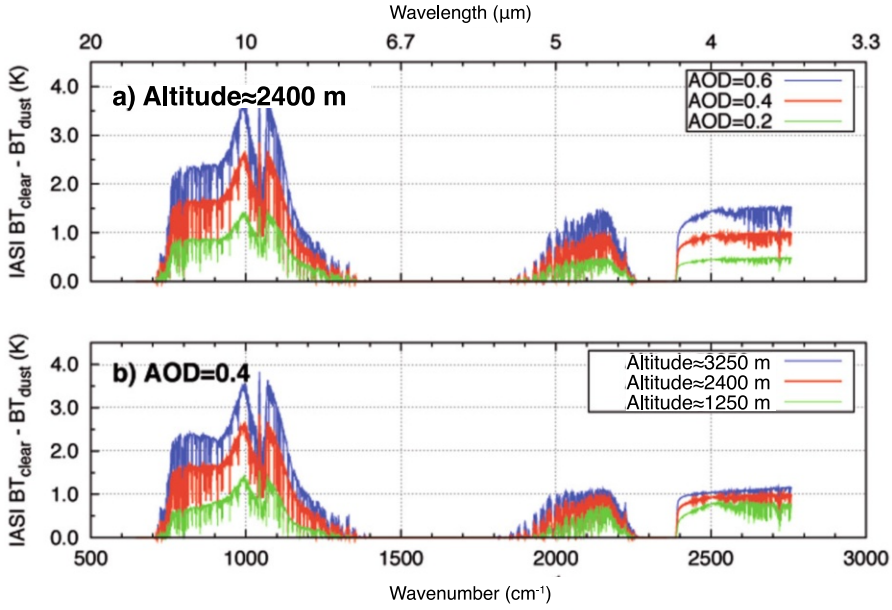

Figure 9.18 Simulated impact of dust AOD (top) and altitude (bottom) on IASI brightness temperature spectra over oceans, by night (courtesy of S. Peyridieu).

clouds, which are usually bright over dark surfaces in the shortwave, may benefit from visible reflectance observations, if available.

Amongst cloud masks used for aerosol remote sensing applications, there are threshold tests (usually, a BT difference between 2 channels that must be higher or lower than a threshold), spatial heterogeneity tests or tests using exogenous data (from other instruments).

The aerosol signature on the infrared spectrum shows a typical "V-shape" observed by many authors, e.g. Sokolik (2002) for dust, or Karagulian et al. (2010) for ash. This is also sometimes referred to as "negative slope" in the 800–1000 cm^{-1}, in contrast to the positive slope observed for cirrus clouds (see Figure 9.19). This effect makes it possible to distinguish clouds (especially thin cirrus) from aerosols using a threshold test. Radiative transfer simulations can help to find couples of channels which are well correlated over a wide range of atmospheric situations except cloudy ones. If the difference between these channel BTs reaches a given threshold, the pixel is flagged as cloudy. In order to prevent a pixel being flagged as cloudy when dusty, the dust effect must be different from the cloud effect. For instance, if the presence of clouds decreases the difference between two channels, the presence of dust should increase this difference or keep it constant. This technique has been used for AIRS by Pierangelo et al. (2004b).

An example of exogenous data is the use of microwave sounder measurements (for example, the AMSU instrument, on board the same satellites as AIRS or IASI). Microwave radiances are not sensitive to most clouds and can be used to predict an infrared radiance or brightness temperature. When the predicted infrared BT is too far from its measured value, the pixel is considered as cloudy. Another example: for the IASI infrared sounder, it is possible to use the cloud mask from the AVHRR imager.

The spatial heterogeneity tests rely on the spatial difference between aerosols (usually forming homogeneous plumes or "clouds") and water or ice clouds which are more heterogeneous. For such a test, one considers that the standard deviation between neighbor pixels must be lower than a given threshold in order for these pixels to be considered cloud-free.

Several approaches are generally combined together. For example, Hansell et al. (2007) combined, for the MODIS instrument infrared channels, the simple difference in the threshold technique with a double difference ("slope method") and analytical expression including a BT difference and visible reflectance ratios.

Removing the "calculated minus observed" biases

Radiative transfer models often show a bias with observed measurements. This systematic bias can come from the model (e.g. a spectroscopy error) or from the instrument (e.g. calibration uncertainty or poor knowledge of the response function). Since the retrieval often relies on simulated data, their application to real data implies that any brightness temperature systematic biases between simulations and observations have been eliminated. This correction is of particular importance for climate applications. This "calculated minus observation", also called "calc-obs", bias is routinely monitored in operational weather forecast centers. For aerosol remote sensing applications, these biases might be evaluated by comparing simulations and observations for a set of collocated satellite observations and radiosondes (e.g. ERA 40) or NWP analyses, for example from the European Center for Medium-Range Weather Forecasts, for clear sky situations. By adding the average bias (calculated – observed), the observed BT are scaled to the radiative transfer model BT reference frame. The biases usually distinguish night and day, land and sea, and sometimes latitude bands. This procedure also prevents the background aerosol, whose loading shows a weak temporal variability, from contaminating the retrieval.

9.4.3 Detecting aerosols

The signature of a strong aerosol event (desert dust, volcanic ash, etc.) on an atmospheric spectrum is usually easily detected "by the naked eye" on a full infrared spectrum, thanks to the previously mentioned "V-shape". However, this signature greatly depends on the atmospheric and surface states. Contrary, therefore, to retrieving dust properties, i.e. producing a well-defined physical parameter (e.g. the AOD at a given wavelength), detecting dust can be performed via simple algorithms, like two channel BT differences. The combination of more channels is also possible, but the principle remains similar: some of the channels are not sensitive to aerosols and are used to estimate the "base-line" while the other channels have decreasing BT when the aerosol load increases. The selection of the channels can be performed through radiative transfer simulations or by comparing spectra with or without an aerosol plume. These algorithms are widely used, both for radiometers

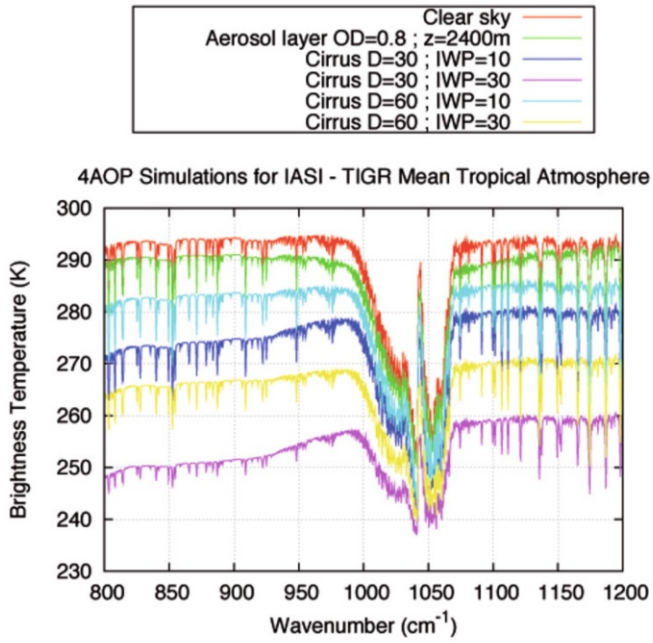

Figure 9.19 Comparison of the effect of aerosol and cirrus clouds on the infrared spectrum from 800 to 1200 cm^{-1} (8.3 to 12.5 μm). The diameter D and Ice Water Path (IWP) of cirrus models are given in the legend at the top. Simulations over ocean.

and spectrometers (e.g. Ackerman, 1989; Wald et al., 1998; De Souza-Machado et al., 2006; Karagulian et al., 2010, etc.). Their advantages are their simplicity and a very fast computation time, suitable for near-real time. These algorithms are very useful to track aerosol plumes, for the monitoring of air quality for example. However, they do not give access to a geophysical quantity (such as mass or AOD), and they can be applied only for case studies as they might suffer from regional biases. For instance, the BT difference can also be sensitive to the Earth's surface emissivity or temperature. In order to bypass these difficulties, more sophisticated linear regressions are possible, when introducing for example exogenous data for the surface temperature.

As an illustration, Figure 9.20 shows that the difference between HIRS (the High Resolution Infrared Sounder on board the NOAA satellites) channel 8 (11.1 μm) and channel 10 (8.3 μm) depends almost linearly on the surface temperature. So, Pierangelo et al. (2005b) introduced the regression residual r

$$r = BT(10) - BT(8) - \left(aT_{surf} + b \right), \tag{9.25}$$

where the linear regression coefficient a and b are determined on a clear-sky data set (either from simulations or from observations). The bottom plot of the same figure shows that this regression residual is almost insensitive to the clear-sky atmospheric variability (including water vapor content). Consequently, any departure of r from 0 comes from the presence of an aerosol, which was not included in the regression data set. Since the effect of aerosols on the BT is higher at 8.3 μm than 11.1 μm, the value of r increases with the aerosol load. However, the exact relationship between the residual r and the AOD strongly depends on the aerosol altitude, this is why this algorithm is suitable for detection only but not for the retrieval of optical depth[3].

Another example is the detection of dust over deserts with geostationary satellites: the high number of observations for a given area can be used by algorithms working with a clear and dust-free reference image. For each pixel, the reference BT at a fixed time is the highest BT observed during a period typically lasting half a month. The time period must be long enough to allow clear-sky day(s) and short enough to consider the emissivity of the Earth's surface as locally unchanged. The drop of observed BT with respect to the reference is associated with the presence of dust, both because of its direct effect on the radiation and because of the decrease in surface temperature mainly due to the shortwave irradiance decrease. Legrand et al. (1985) introduced this technique and later Legrand et al. (2001) built an Infrared Difference Dust Index (IDDI) over the Sahara using Meteosat observations.

Dust presence results in a change of outgoing radiance at TOA, arising from the difference between the skin surface temperature and the temperature of the dust layer above giving rise to a *thermal contrast method* (according to King et al. (1999)). In the daytime, the land surface is hotter than the dust, especially in arid regions. The hotter the surface, the stronger the thermal contrast and the radiance deficit at TOA. So, dust detection is performed in the middle of the day (at 12:00 UTC for Meteosat observing Africa).

A simple analytic expression of the dust-induced radiance deficit at TOA is possible with the following assumptions: (i) absorbing gases are not considered; (ii) the surface is assumed black at temperature T_s with no impact of dust on it; (iii) dust is assumed non-scattering; (iv) the dusty layer is assumed isothermal at T_d, with a transmittance t; (v) the spectral integration throughout the channel bandpass width is ignored. The radiance measured at TOA is then

$$L_{sat} = tB(T_s) + (1-t)B(T_d), \tag{9.26}$$

with B the black body (Planck) function for Meteosat channel. The TOA radiance deficit is thus the difference between the TOA radiances without and with dust

$$\Delta L_{sat} = (1-t)\left[B(T_s) - B(T_d)\right]. \tag{9.27}$$

3 A second linear regression using HIRS channel 18 (at 4.0 μm) and channel 10 shows a different sensitivity to altitude and AOD. Combining both regressions gives the possibility to disentangle AOD and altitude.

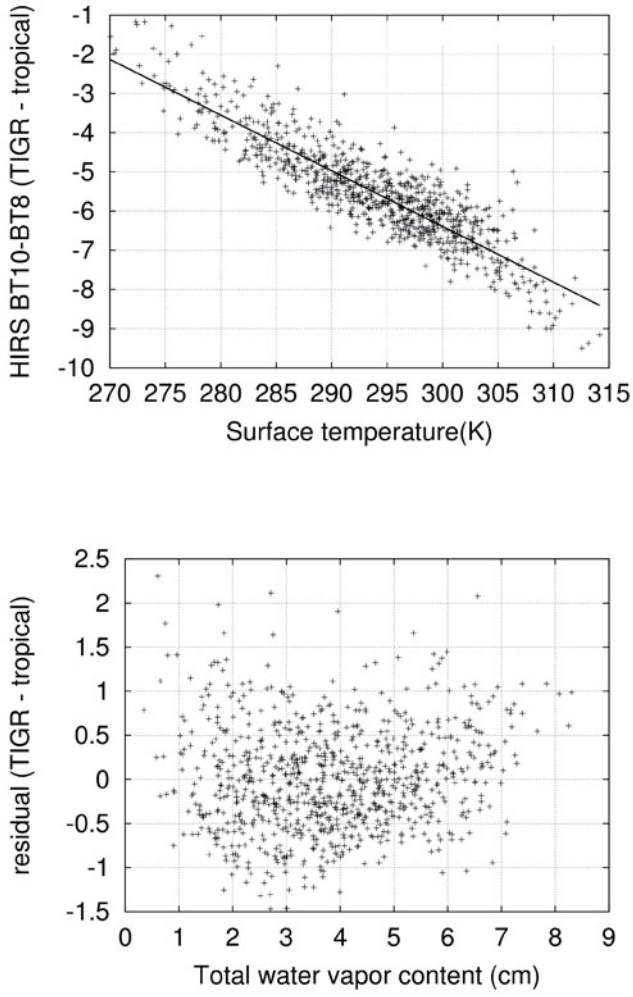

Figure 9.20 Top: difference in calculated brightness temperature between HIRS channel 10 and channel 8 as a function of sea surface temperature for a data set of clear-sky tropical atmospheres from the TIGR database. Bottom: residual of the linear regression between the two channels BT and the surface temperature as a function of total water vapor content.

The transmittance t depends on the amount of dust and its optical properties through the TIR AOD, while the thermal contrast $(B(T_s) - B(T_d))$ depends on the skin surface temperature and on dusty air temperature.

For an arid surface, solar energy is absorbed during daylight and mostly confined within a thin superficial layer. This enhances the skin surface temperature T_s and creates a strong superadiabatic lapse rate in the first meters over the surface of up to 60 K/m, interpreted as a temperature discontinuity at the surface (15–20 K at noon, from measurements near Niamey; Frangi et al., 1992). A consequence is that the IDDI – i.e. the TOA radiance or BT deficit – will be high where the discontinuity of temperature at the surface is large, i.e. over the dry bare ground of the arid and semi-arid regions, these very regions where sources are located and from where dust is emitted. There, the satellite signal will be large, even if dust lies in the surface boundary layer (as it usually does). On the contrary, vegetated surfaces and water bodies will experience little or no discontinuity (due to evaporation and evapotranspiration processes), resulting in a weaker sensitivity to dust (in the latter circumstances dust can be detected at high altitude only).

Illustrations of such detection algorithms are given in Section 9.5.

9.4.4 Direct retrieval

Herein we refer to the inversion from the infrared measurement of a geophysical quantity related to the aerosol (typically its optical depth, but it could also be its total mass, size distribution, altitude, etc.) as "retrieval". We refer to an inversion process where no precomputed brightness temperature data are used and no radiative transfer code is used during the retrieval as "direct retrieval".

The retrieval can rely on a direct relationship between an aerosol property (e.g. AOD) and a function of brightness temperatures. Such a relationship can be established empirically or on the basis of extensive simulations. This approach is widely used for broadband instruments. As an example, the dust loading is retrieved from SEVIRI using a linear combination of channel BTs (Brindley and Russel, 2006).

9.4.5 Physical retrieval

A second family of retrieval algorithms is based on a fit between observed radiances and calculated radiances given by a radiative transfer code. A radiative transfer computation is thus needed for each single processed spectrum. The fit is performed, for instance, by finding the aerosol characteristics and sometimes other parameters such as the temperature profile or Earth's surface state, that minimize a distance, generally a χ^2 type distance. The elements to fit must include all the parameters that are not supposed to be known. For measurements from a spectrometer, this technique has the advantage of using the full spectrum. The Bayesian approach described in the book from Rodgers (2000), known as "optimal estimation", is widely employed for vertical profile retrieval of temperature or gases.

The state vector x, containing all the unknowns, is related to the measurement vector y through the equation

$$y = F(x) + \varepsilon, \tag{9.28}$$

where ε is the measurement noise.

The inverse problem is solved by iterative linearization

$$y = Kx + \varepsilon, \tag{9.29}$$

where K is the Jacobian matrix that contains the partial derivatives of y with respect to the elements of x.

Since this inverse problem is under-constrained, it has to be regularized. This can be done using various methods, such as via Twomey-Thikonov regularization, or Bayesian regularization. Bayesian regularization introduces the *a priori* state vector x_a, the *a priori* covariance matrix of the state vector, S_a, and the noise covariance matrix, S_ε and it can be shown that the most probable state vector, i.e. the best estimate of x, is given by

$$x = x_a + \left(K^T S_\varepsilon^{-1} K + S_a^{-1}\right)^{-1} K^T S_\varepsilon^{-1}\left(y - F\left(x_a\right)\right). \tag{9.30}$$

Since the problem is usually moderately nonlinear, it is in fact solved by successive iterations.

The optimal estimation approach has been tried for aerosol retrievals (Clarisse et al., 2010) for intense events where it may be preferable to study the gas and aerosol chemistry together. Although this technique theoretically brings the lowest uncertainty on the retrieved quantity, it is very time-consuming (an iterative scheme with a call to the RTE at each loop is required, including the computation of partial derivative with respect to aerosol and gases), even when using a simplified scheme for the RTE (Kruglanski et al., 2006). The theoretical bases for this approach require the problem to be sufficiently linear and the distribution of errors and parameters to follow Gaussian distributions. The dependency of the result on the first guess and the *a priori* knowledge might be a drawback of this method.

9.4.6 Look-up table retrieval

As radiative transfer computation is often very time consuming, the inversion of a very high number of observations for global applications often requires a look-up table (LUT) approach. This technique is very similar to the previous one, except that the simulated BTs for the fit are not calculated for each retrieval. They are instead calculated in one go for a large and representative set of situations (surface, atmosphere, aerosol, observation geometry, etc.) and stored in the so-called LUT. The distance to minimize generally looks at observed and simulated BTs but also BT differences between two channels, the differential aspects adding a constraint on the proximity recognition. A typical distance for i selected channels and j independent selected couples is

$$D = \sum_i \frac{\left(BT_i^{calc} - BT_i^{obs}\right)^2}{\sigma_i^2} + \sum_j \frac{\left(\Delta BT_j^{calc} - \Delta BT_j^{obs}\right)^2}{\sigma_j^2}, \tag{9.31}$$

where σ_i^2 is the variance of the calculated BT_i over the whole LUT. This normalization is necessary to put the same weight on each selected channel.

Even though the generation of the LUT is time consuming, its application is straightforward. The retrieval consists of computing the distance D between the observation and all the situations in the LUT, or a subset of situations in the LUT if some *a priori* information is known (like, obviously, geometric knowledge as the viewing angle, or the thermodynamic state of the surface or the atmosphere from a first-step retrieval). Then, the situation of the LUT that minimizes the distance D is chosen and gives the desired aerosol properties. More sophisticated selection of several "minimal" situations can be combined (e.g. Peyridieu et al., 2010a), in order to take into account the noise of the individual measurements, for instance.

As an example, the LUT calculated for the retrieval of dust AOD and altitude from AIRS by Peyridieu et al. (2010a) has been built by computing the brightness temperatures for each of the eight selected channels, for the 567 atmospheric situations from the TIGR dataset, for seven viewing angles (0 to 30°), for nine dust AODs (0.0 to 0.8), and for eight mean altitudes of the layer (750 to 5800 m).

Validating the LUT retrieval is an indispensable step. As the full inverse problem is ill-posed, it is necessary to check that the parameterization applied (i.e. the choice of the quantity to retrieve and the channel selected) is sufficient to avoid multiple solutions or zero solutions. The discretization of the variability of the atmosphere through the choice of the thermodynamic profiles and the aerosol parameters must also be checked. This validation can be performed easily through the application of the retrieval algorithm to each simulation of the LUT, removing, of course, the tested situation itself from the LUT when looking for the minimum distance.

Once the LUT is built, instead of minimizing a distance, it should be theoretically possible to educate a nonlinear regression algorithm, such as a multilayer feed-forward neural network. Neural networks have been used for trace gas retrievals (e.g. Chédin et al., 2003; Turquety et al., 2004; Crevoisier et al., 2004), but, as far as we know, not for aerosol retrieval.

9.4.7 Specificities of a retrieval algorithm over land

The capability of detection of aerosols over land (especially dust or ash in the coarse mode) is an advantage of the longwave, compared with the visible domain. In the shortwave, the contrast between the reflectance of the ground and the reflectance of the aerosol layer is sometimes too low (over high albedo surfaces such as deserts) and prevents both signals from being disentangled. This is one of the great assets of using the longwave domain for aerosol remote sensing. Nevertheless, remote sensing of aerosol from infrared observations above land surfaces remains tricky.

As seen before in Section 9.3, the Earth's surface emission depends on surface temperature and emissivity[4]. Over the oceans, the surface emissivity is well known and almost constant spectrally, close to 0.99 at 10 μm, slightly depending on the incident angle. Some tables provide the spectral and directional dependency of sea water (Masuda et al., 1988).

4 Note that, in addition to surface emissivity, for a retrieval over land the ground altitude of the observed point must also be taken into account through the surface pressure but this usually does not present any difficulty.

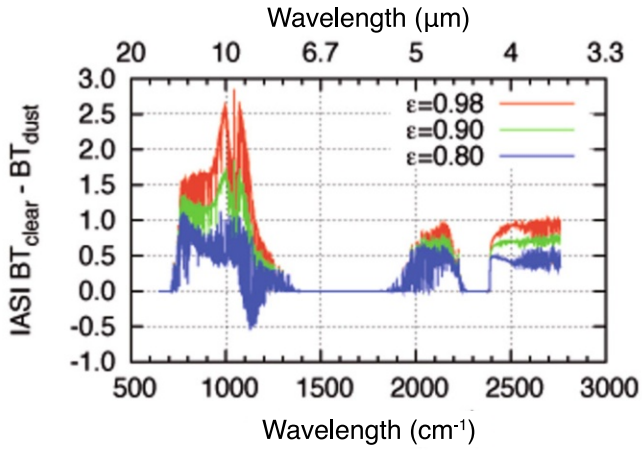

Figure 9.21 Simulated effect of surface emissivity on the BT difference (clear – dust) for IASI channels (AOD=0.4, altitude=2400 m).

However, over continental surfaces, the emissivity is spectrally, spatially and temporally variable. The infrared surface emissivity depends on many parameters: the composition of soil (type of mineral or vegetation), its moisture, and its roughness (Salisbury and d'Aria, 1992). Moreover, the spectral and angular variations of emissivity are significant (e.g. Salisbury and d'Aria, 1992 ; Péquignot et al., 2008). Over bare soils or deserts, the surface emissivity might reach values as low as 0.7 at 8.5 μm. Over semi-arid lands, like savannas, the seasonal cycle of emissivity is significant (Chédin et al, 2004) because of the change in the vegetation influenced by seasonal precipitations. This variability has an influence on the radiation emitted and modulates the aerosol impact (Figure 9.21) as noted by Legrand et al. (2001). This comes directly from the change in the radiation emitted, but also from the energy exchange between the atmosphere and the surface which modulates the surface temperature (Legrand et al., 1992). Note that the ground is always supposed Lambertian with respect to its infrared emissivity. This is a sensible hypothesis, given the large size of satellite sounder footprints.

For aerosol remote sensing over land, there are two main possibilities: the emissivity might be taken from exogenous data, or be by-passed by an adequate choice and combination of channels.

Regarding the first possibility, the knowledge of surface emissivity might come from a prior retrieval with the same infrared observations. The dust detection by a regression algorithm for HIRS channels by Pierangelo et al. (2005b) is extended over land by using the monthly averaged surface emissivity from Chédin et al. (2004). Their emissivity retrieval is based on the assumption that the emissivity varies slowly over time, contrary to surface temperature. De Paepe and Dewitte (2009) used the algorithm described in Minnis et al. (2002) to retrieve the surface emissivity from SEVIRI channels before retrieving mineral

dust aerosol. Knowledge of surface emissivity may also come from another instrument with similar channels: Li et al. (2007) used MODIS infrared surface emissivities as input for their Saharan dust retrieval algorithm applied to SEVIRI. In some cases, for example when the knowledge of the surface material is sufficient, surface emissivity might be also taken from a library: let us mention the MODIS/UCSB and ASTER/JPL emissivity libraries which archive very high spectral resolution laboratory measurements of the emissivity of different samples of typical Earth surfaces. They can be downloaded from the Internet (http://www.icess.Ucsb.edu/modis/EMIS/html/em.html and http://speclib.jpl.nasa.gov/ respectively).

The second possibility might consist of a difference in brightness temperatures selecting channels for the baseline close to 12 μm, where the emissivity is almost constant with respect to the soil type (Péquignot et al., 2008). It is also implicitly used by algorithms selecting only channels at wavelengths where the surface emissivity does not vary too much. For that reason, Li et al. (2007) do not use the 8.7 μm channel of SEVIRI.

A third possibility would be to retrieve aerosol and surface properties simultaneously, but this increases the number of parameters to retrieve and would almost certainly lead to difficulties, as emissivity or surface temperature and aerosol effects can compensate each other.

The capability of infrared measurements to remotely sense the aerosol over land surfaces depends on the application: extreme event study or long-term climatologic observation. For a local case study, limited to a small region of desert for example, the emissivity might be indeed adjusted or assumed to be known and/or spatially constant. However, for global retrievals or for long-term climatology, this is far more complicated as the surface emissivity might be the cause of regional or seasonal differences in the retrieved aerosol characteristics. To our knowledge, no truly global data set of aerosol loads obtained from infrared measurements has been built: retrievals either work over the ocean only, or are limited to regional areas with one surface type, like the Sahara desert at the maximum.

9.4.8 Validating and comparing the results

Validating an aerosol product retrieved from a longwave instrument is not an easy task. The optimal way to validate the retrieved AOD would be to compare it with direct measurements, but "direct" observations of TIR optical depth routinely measured from the ground still do not exist. The few direct observations of longwave radiation from the ground (see Section 9.5.2) provide radiances (or BT) containing information on aerosol amounts, "weighted" with the aerosol properties (including aerosol altitude, particle size and composition) and depending on the thermodynamic state of the atmosphere. So AOD retrieval is difficult and will result in significant uncertainty if the aerosol properties and the state of the atmosphere are unknown.

Comparing aerosol products retrieved from infrared measurements with data from the on-ground sun-photometer network AERONET is not straightforward and raises several issues:

(i) the relationship between the visible or shortwave AOD and the longwave AOD depends on the aerosol particles composition, size and shape, which are usually

unknown, and can render the comparison irrelevant: the photometer and infrared sensor are not sensitive to the same particles.

(ii) the aerosol content might change rapidly with time over a given station, which implies that night-time retrievals can not be validated this way.

(iii) AERONET retrievals over some stations are available only 2–5 days each month (because of the cloud cover), and this may not be suitable for a comparison with satellite-based products given for a wider area or averaged over a longer period. The comparison with single satellite pixels also suffers from the time difference, reinforced by the sparseness of the data because of the clouds.

While the comparison of the aerosol optical depth is not always relevant, the effective radius of aerosols retrieved from infrared observations can be interestingly compared with the AERONET retrieval of the coarse mode effective radius, which is computed for both spherical and nonspherical particles. However, some of the previously mentioned difficulties remain (the time difference in particular).

Longwave aerosol products can be compared with other satellite-based products, on the basis of spatio-temporal variability analysis. It has the advantage of a global approach. Even if this type of comparison is not an exact validation, it is nevertheless very useful, not only for increasing the confidence in the new aerosol product, but also for exploiting the synergy between sensors and highlighting some interesting geophysical behaviour. However, as reported by Mishchenko et al. (2007) and Liu and Mishchenko (2008), comparison of aerosol datasets from different satellite-based instruments still represents a challenge.

Infrared sensors that might be exploited for aerosol retrieval are not as widespread as visible sensors. Consequently, the comparison between two infrared AODs is not always possible. Peyridieu et al. (2010b) have compared the Saharan dust AOD over ocean from IASI and AIRS, but this is to our knowledge the only example of direct comparison of two similar infrared products (even if the time pass difference implies that the diurnal cycle of dust is not sampled by the two spectrometers in the same way).

Comparisons of satellite-based IR and visible aerosol products will identify similar patterns of dust clouds, but we expect differences between the two classes of products:

- The visible AOD is sensitive to particles in the accumulation and coarse mode, which implies that visible AOD products detect not only dust but also smaller particles such as biomass burning aerosol, pollution aerosols, etc.
- The infrared and visible wavelengths are sensitive to different particle size, therefore the ratio of IR to visible AOD depends on the PSD, which is modified during transport by gravitational settling (Maring et al., 2003). See for example Figure 9.22.
- The ratio of IR to visible AOD depends on the mineral composition in the case of dust, which in turn depends on the geographic origin (source of the aerosol cloud).
- The time difference is often a critical issue for elementary comparison, as visible retrievals need a high solar zenith angle while infrared retrievals usually prefer night data. This is why comparisons over longer time periods, e.g. monthly means, are preferred.

- The space sampling also differs: infrared sounders, for instance, have round footprints with a diameter of the order of 10 km (3 km for Meteosat Second Generation), while visible imagers have smaller square pixels.

As a consequence, visible and infrared AOD must not be considered as equivalent products which could be converted into each other but rather as fully complementary products whose comparison opens the way to very promising studies.

Until recently, the IR-retrieved altitude of dust (related to the temperature of the layer) was very difficult to compare, as only a few in-situ or ground-based lidar observations from campaigns were available. It can now be compared with the CALIOP lidar data on board the CALIPSO satellite (Winker et al., 2009), even if the space sampling is extremely different. The lidar has a high horizontal resolution (5 km for CALIOP level 2 product) for detecting aerosol features. However, CALIOP only carries out nadir measurements, and so its coverage is much poorer than a scanning instrument like AIRS due to the distance between two successive orbits (more than 1000 km). This is why comparing CALIOP and AIRS products is not straightforward. Peyridieu et al. (2010a) consequently made comparisons between AIRS and CALIOP on the basis of their respective monthly means. They also have chosen to select cases for which only one aerosol layer is detected and measured by the lidar. This procedure also avoids computing an "average" altitude from various lidar layers with different composition or microphysical properties, which could not be

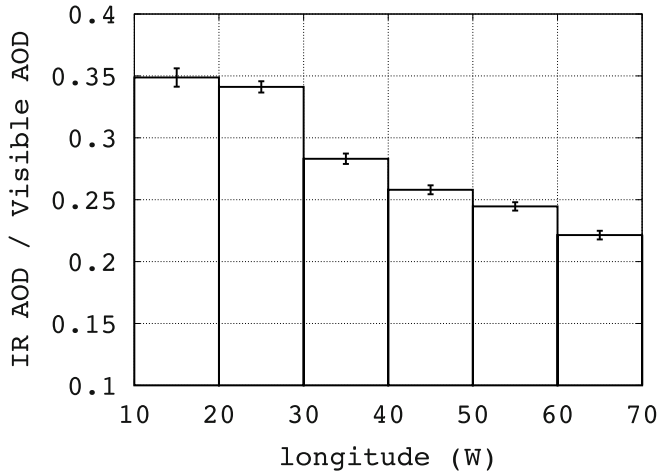

Figure 9.22 Ratio between the AIRS retrieved 10μm AOD and the MODIS retrieved 0.55μm AOD, for July 2003, for 0-30°N, as a function of longitude (from the African coast to the Caribbean sea). From Pierangelo et al. (2004b).

compared with AIRS equivalent altitude, as the infrared effect of these layers might change deeply with composition or properties, especially the median size of particles.

Aerosol products retrieved from infrared observations can also be compared with aerosol characteristics taken from chemistry and transport models (e.g. LMDz-INCA, described in Hauglustaine et al. (2004)), but model representations are still imperfect (vertical transport is still rather coarse, for instance) and the extrapolation of geophysical quantities to optical quantities (e.g. from total mass content to AOD or from mass median diameter to effective radius) usually requires some additional hypotheses.

9.5 Illustrations

9.5.1 Space observations

May we first remind readers that none of the infrared instruments on board satellites were originally designed for aerosol remote sensing. For example, the infrared sounders, HIRS or IASI, are operational instruments dedicated firstly to the retrieval of temperature and humidity profiles in the atmosphere for weather forecast applications. Similarly AVHRR, Meteosat and MSG/SEVIRI, are all meteorological instruments.

Moderate spectral resolution radiometers

Radiometers (or band instruments), as opposed to very high spectral resolution spectrometers, have been flown on board satellites for decades. The NOAA meteorological low Earth orbit satellites have been continuously carrying the infrared sounder HIRS and the imager AVHRR (with both visible and infrared window channels) since 1979. The geostationary Meteosat satellites have been offering observations in the longwave domain since 1981 (re-analysis of the archive by EUMETSAT). The long-term records make the retrieval of aerosol properties from these instruments extremely valuable for climate studies.

The first detection of dust using infrared observations was obtained from these instruments through brightness temperature differences or simple linear regressions. The potential of thermal infrared for monitoring mineral dust events has been investigated focusing on case studies (e.g. Ackerman, 1989; Wald et al., 1998) using data from NOAA/HIRS (High resolution Infrared Radiation Sounder). An 8-year climatology of a dust index over land in the tropical zone has been retrieved from HIRS (Pierangelo et al., 2005b), showing significant seasonal variations of dust sources. As an illustration, Figure 9.23 shows the location of the sources of dust over the Sahara, active for the month of April, from 1988 to 1991.

Following the Pinatubo eruption in June 1991, volcanic aerosols were also widely studied from infrared sounder measurements. Baran et al. (1993) analyzed the effect of Pinatubo aerosols on differences in brightness temperatures from HIRS-2 using in-situ observations of aerosol particle size and number density. They suggested retrieving the aerosol mass loading from this BT difference. Ackerman and Strabala (1994) or Pierangelo et al. (2004a) used three brightness temperatures (at 8, 11, and 12 μm from HIRS-2) to retrieve their vis-

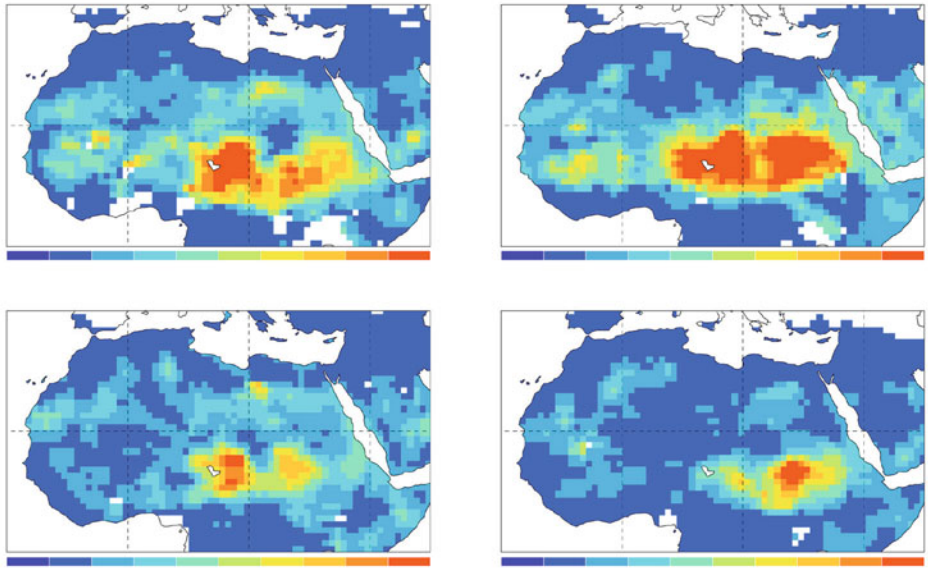

Figure 9.23 Dust index from NOAA/HIRS over the Sahara for the month of April, from 1988 (top left) to 1991 (bottom right). The activity of the sources over Tchad are clearly visible, together with some inter-annual variability. From Pierangelo et al. (2005b).

ible and infrared optical depths. The limitation of these instruments is the small number of broadband channels, which restrains the number of aerosol parameters that can be retrieved and sometimes implies some contamination by trace gases (water vapor or ozone).

Dust detection using geostationary TIR images

The Infrared Difference Dust Index (IDDI) (Legrand et al., 2001) is a Meteosat-derived TIR index dedicated to remote sensing of desert aerosols over land (using the former Meteosat First Generation series with a single IR channel at [10.5–12.5 μm]). The IDDI product proved to be efficacious in studies of dust source location and seasonal activity (Brooks and Legrand, 2000; Léon and Legrand, 2003; Deepshikha et al., 2006a, b). Figure 9.24 shows seasonal IDDI means over Africa calculated throughout the period 1983–98. The structures with high mean IDDI values indicate large atmospheric dust loadings, revealing the active sources of dust emission. This dust index has been used also for the study of the physics of dust emission (Chomette et al, 1999; Marticorena et al., 1997, 1999, 2004), for the description of dust transport (Petit et al., 2005), for the determination of the dust mineral composition with respect to its source of emission (Caquineau et al., 2002) and for meteorological dust forecasting (Hu et al., 2008). Figure 9.25 shows the distribution

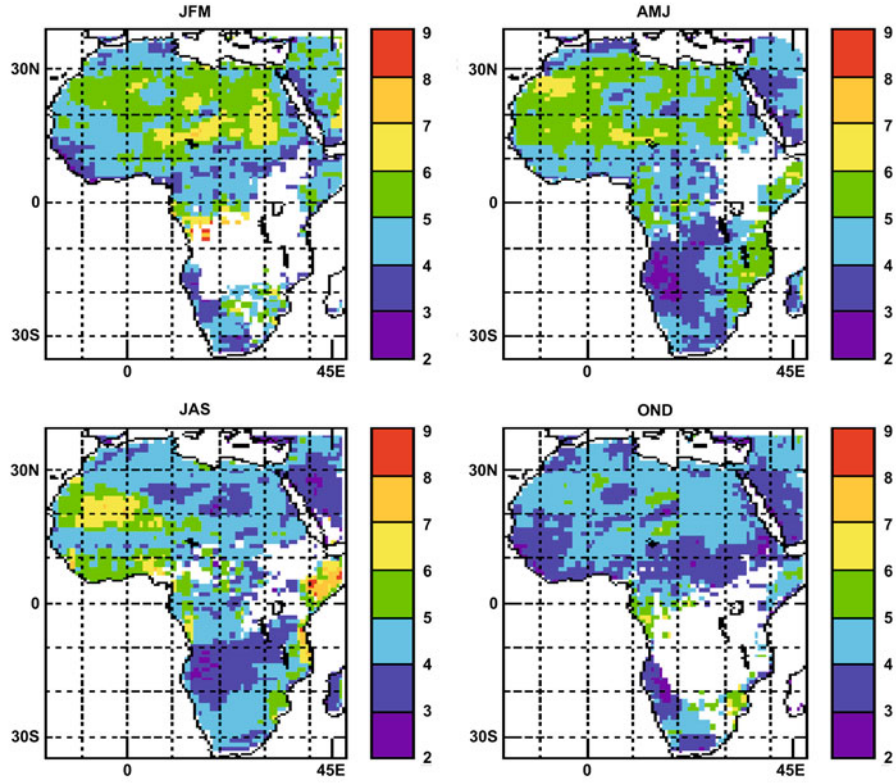

Figure 9.24 Seasonal dust climatology over Africa for the period 1983-1998, represented by 3-month mean fields of IDDI values (in K) on a 0.5°×0.5° grid. White areas are those where cloud presence is frequent.

of dust over China and the corresponding sources, derived from an operational dust detection algorithm generating IDDI and using the data from the meteorological geostationary satellite FY-2C.

Very high spectral resolution sounders: AIRS, IASI

The new generation of sounders (AIRS and IASI) offers a higher number of channels: more aerosol properties can be retrieved from radiance measurements, and the deconvolution of variable gases and aerosol effects is easier, due to the very high spectral resolution. These high performances have also enlarged the number of applications of aerosol products retrieved from infrared observations, as for example the monitoring of aerosols for air quality or the monitoring of volcanic activity for air traffic.

Soon after its launch in 2002, studies demonstrated the ability of AIRS observations to monitor clouds and volcanic aerosol (Ackerman et al., 2004; Carn et al., 2005), or Saharan

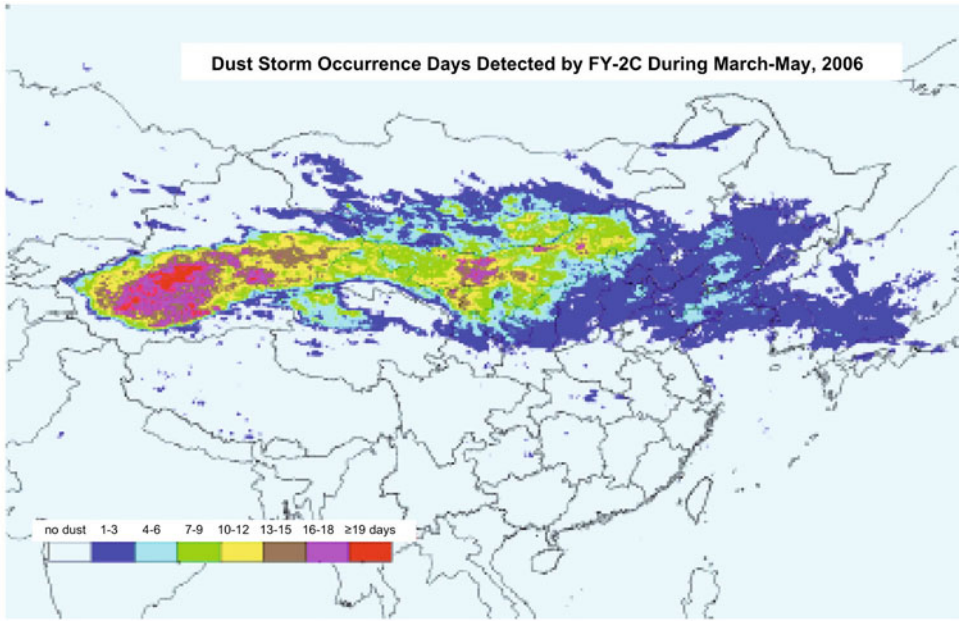

Figure 9.25 Dust occurrence frequency over eastern Asia derived from the geostationary satellite FY-2C (adapted from Hu et al., 2008).

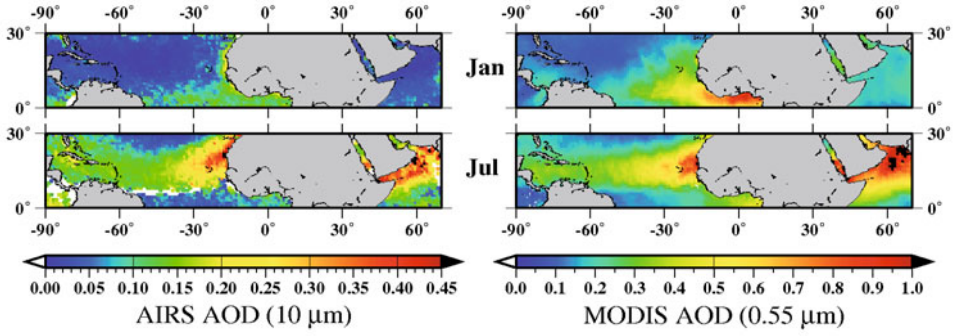

Figure 9.26 6-year (2003–2008) climatology of monthly AOD. Left: 10 μm AOD from AIRS; right: 0.55 μm AOD from MODIS. From Peyridieu et al., 2010a.

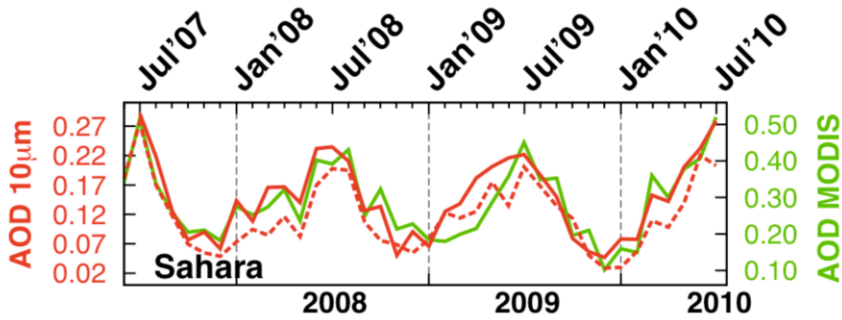

Figure 9.27 Seasonal variability of Saharan dust AOD over the Atlantic Ocean close to the Sahara (10–35°W, 0–28°E): the infrared AOD is retrieved from AIRS (red dotted line) and IASI (red thick line) and compared with MODIS AOD at 0.55 μm (green line). (Courtesy of S. Peyridieu).

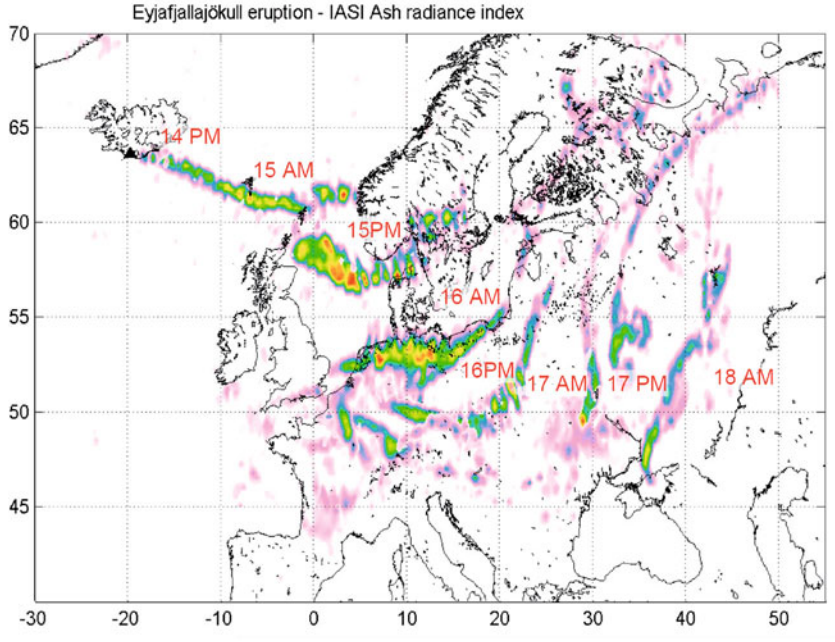

Figure 9.28 Composite image of the ash cloud in the days following the Eyjafjallajökull eruption, in April 2010. The ash radiance index is obtained by a difference between channels. (Courtesy of L. Clarisse.)

dust (Pierangelo et al., 2004b; de Souza-Machado et al., 2006). A tropical climatology of dust (infrared AOD and altitude) has been derived from AIRS for almost eight years (2003–2010) (Peyridieu et al., 2010a). The comparison with MODIS visible AOD gives access to added-value information, like the sedimentation of dust during transport, or the distinction between dust and biomass burning aerosols. It is clearly visible in Figure 9.26 that the aerosol over the Atlantic ocean is mainly composed of dust in summer, while biomass burning aerosols, not seen by AIRS, are predominant in winter. The aerosol layer altitude compares well with the CALIPSO lidar products. The effective radius of dust is also a parameter that can be retrieved in a second-step retrieval (Pierangelo et al., 2005a).

The first results from the IASI instruments, launched in 2006, are very promising. Saharan dust detected with IASI shows a seasonal cycle very similar to the one observed with AIRS, as can be seen on Figure 9.27. The capability of IASI to detect volcanic ash aerosols is reported by Gangale at al. (2010). An illustration for the monitoring of the Eyjafjallajökull ash cloud is shown on Figure 9.28.

Limb observations

Limb observation of the infrared emission of the atmosphere can also provide the extinction profile of volcanic aerosols. Note that the lower part of the atmosphere, becoming progressively too opaque, cannot be observed with a limb sounder, which restricts their use to high altitude aerosols (above 7–8 km), i.e. upper tropospheric and stratospheric aerosols. Lambert et al. (1993) studied Pinatubo aerosol using satellite observations in the infrared range from the Improved Stratospheric and Mesospheric Sounder (ISAMS). They retrieved area-weighted mean stratospheric optical thickness at 12.1 μm on a global scale from the zonal mean extinction profiles. The Cryogenic Limb Array Etalon Spectrometer (CLAES) instrument made measurements of the infrared emission of stratospheric aerosols near 12 μm from October 1991 until May 1993. Mergenthaler et al. (1995) obtained the aerosol distribution of absorption cross-section, optical depth and sulfuric acid mass estimates with CLAES measurements. Lambert et al. (1997) combined CLAES and ISAMS to retrieve aerosol composition, volume and area mass density. Echle et al. (1998) also determined optical and microphysical parameters of Pinatubo aerosols using the Michelson Interferometer for Passive Atmospheric Sounding, Balloon-borne version (MIPAS-B).

9.5.2 Ground-based observations

First, let us emphasize that there are no routine measurements or network of instruments dedicated to aerosol remote sensing in the longwave, so far. In the shortwave, ground sun-photometers provide an almost direct measurement of aerosol optical depth, because the radiation source (the sun) is observed through the aerosol. Conversely, the longwave observation of aerosol from the ground is indirect: the source is the aerosol itself and the radiance depends first on the aerosol temperature/altitude. Similarly to space observations, the spectrum recorded from the ground mostly carries the information about the thermodynamic state of the atmosphere: temperature, and also humidity. Consequently, the aerosol optical depth in the longwave retrieved from an instrument on the ground needs exogeneous data and contains a non-negligible error and cannot be used for an accurate validation of space-based retrievals.

Even if there is no routine ground measurement of dust in the TIR domain, the CLIMAT radiometer has been used in field campaigns (Sahel, Sahara, China, Guadeloupe).

The CLIMAT instrument (manufactured by CIMEL Company) is a TIR radiometer developed in the 1990s, to be operated from the ground as well as on board aircraft, firstly for analysis and validation of data acquired by space-borne instruments (Sicard et al., 1999; Legrand et al., 2000; Brogniez et al., 2003). This portable instrument measures TIR filtered sky radiance in a wide channel (8–13 μm) and narrow channels 1 μm wide within this window, for the remote sensing of dust. After cloud-contaminated measurements are eliminated, clear-sky radiances are corrected from gaseous (water vapor) contribution in order to provide a dust radiance component. Figure 9.29 (Legrand and Pancrati, 2006) compares time series of clear-sky radiance derived from CLIMAT channel-W measurements, with aerosol AOD at 670 nm and with the columnar water vapor amount from balloon sounding, obtained during the Sahelian campaign NIGER98 at Banizoumbou (AERONET station) during the dry season of 1998. The CLIMAT radiance and AOD signals show very similar coincident peaks during dust events. Figure 9.30, derived from these results, confirms the expected linear relation and the high correlation between CLIMAT radiance and AOD and shows that correction of water vapor variations effect results in a slightly increased correlation. Figure 9.31 compares the IDDI Meteosat signal for Banizoumbou during NIGER98 with the previous aerosol AOD at 670 nm. Again, the IDDI signal shows coincident peaks with the dust optical depth, like in Figure 9.29 with the CLIMAT signal. This is an example of a succession of dust events characterized by the same radiative properties, which means similar mineral composition, size distribution and altitude of transport. The use of back trajectories explains to a large extent such results, indicating low-level transport in the boundary layer and revealing that dust from the observed events at Banizoumbou originated mostly in the Bodele source. Wind-lifted dust events from this source should only have weak variations of size (confirmed with the Banizoumbou AERONET retrievals of particle size distribution) and in composition. So a fixed mineral composition has been assigned to dust, valid for a Sahelian origin according to Caquineau et al. (2002), namely quartz (19%), kaolinite (72%) and illite (9%) and simulations of the measured radiance have been performed using additional information from AERONET particle size retrievals and Niamey Airport radiosoundings. Finally, in Figure 9.32 we can compare the simulated spectral signature of this Sahelian dust in the CLIMAT channels (i.e. the channel sensitivity to dust) with the corresponding signature derived from CLIMAT measurements, after correction of the water vapor effect. A fair agreement is observed between measurements and simulations. A maximum sensitivity is observed for channel N9 covering the spectral region of the Si-O stretch resonance peaks for quartz (around 9 μm) and clays (around 9.5 μm).

Not only radiometers but also spectrometers are used on ground during campaigns to remotely sense the aerosol. For instance, the Atmospheric Emitted Radiance Interferometer (AERI) has been used during the Aerosol Characterization Experiment Asia (ACE-Asia) and the United Arab Emirates Unified Aerosol Experiment (UAE2). Vogelmann et al. (2003) obtained the longwave radiative effect of aerosol during ACE-Asia by removing a simulated clear-sky spectrum. This radiative effect was then converted to an aerosol IR radiative forcing (flux), which is crucial for climate study. However, it is different from an aerosol retrieval as the forcing includes the net surface radiative effects of aerosol amount, composition, size, height and temperature. Similarly, Markowicz et al. (2003) used the

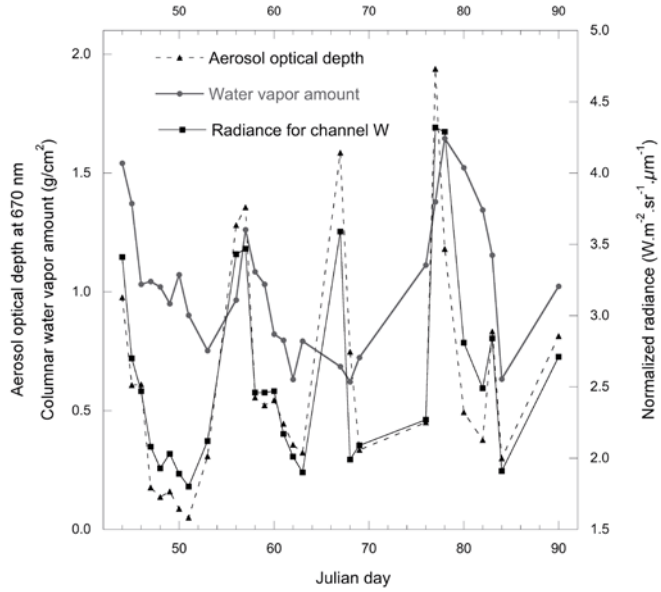

Figure 9.29 For cloud-free days at 12 UTC, 1998, Banizoumbou near Niamey: (i) CLIMAT radiometric measurements (TIR normalized radiance of channel W), (ii) photometric dust optical depth at 670 nm, (iii) water vapor amount from radiosoundings (Niamey Airport).

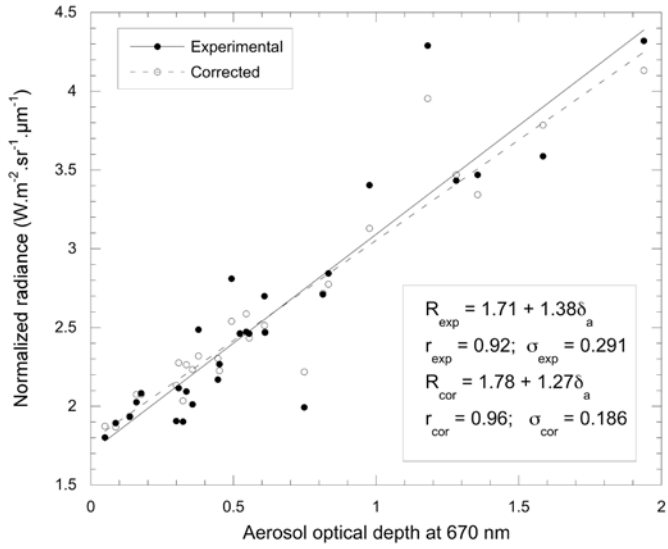

Figure 9.30 Comparison between experimental normalized radiances (for CLIMAT channel W) and the coincident dust optical depth at 670 nm δ_a, before and after correction of water vapor (fixed at 1.03 g/cm^2).

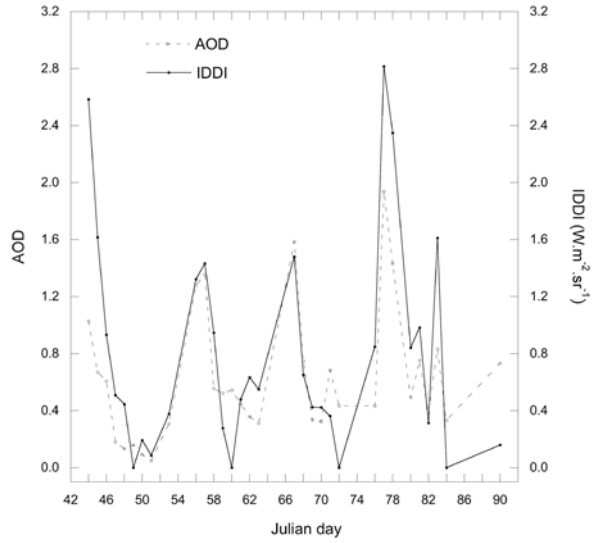

Figure 9.31 Compared temporal series for dust optical depth at 670 nm and IDDI Meteosat in radiance corrected from surface wind effects (Banizoumbou at 12 UTC, same period as in Figure 9.29). The correlation of IDDI with the dust optical depth at 670 nm is r = 0.81. (From Vergé-Dépré et al., 2006.)

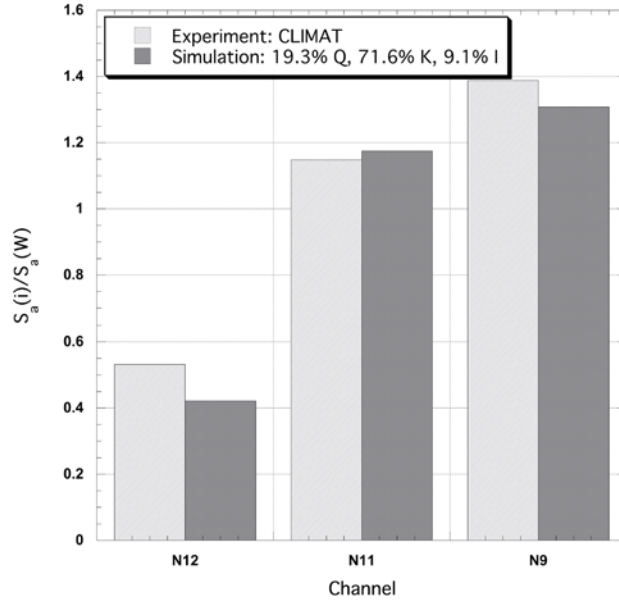

Figure 9.32 Simulated spectral signature of Sahelian mineral dust compared to the CLIMAT-measured signature. These signatures are relative to the wide channel (W) sensitivity to dust (narrow channels are [11.3–12.7 μm] for N12, [10.0–11.1 μm] for N11 and [8.3–9.3 μm] for N9).

infrared spectrometer observations only for computing the aerosol IR forcing and estimated the 10 μm aerosol optical depth from the visible optical depth and an aerosol model. During the UAE2 campaign, aerosol infrared optical depths were retrieved but it was also shown that the characterization of the thermodynamic boundary layer is crucial for accurate dust detection or retrieval (Hansell et al., 2008 ; Nalli et al., 2006). This difficulty is also underlined by FTIR instrument observations during the Lindenberg Aerosol Characterization Experiment (LACE) 1998 campaign (Hollweg et al., 2006). Over all, there is a relatively low number of studies related to aerosol retrieval in the infrared using ground spectrometer, which also emphasizes the remaining difficulties.

9.6 Prospects

The use of the longwave part of the spectrum for aerosol remote sensing is strongly less developed than the shortwave domain. Indeed, the radiative transfer equation in the longwave combines the complexity of absorption and emission by atmospheric gases (water vapor, CO_2, ozone…) and scattering by aerosols. The radiation source is the Earth's surface and atmosphere itself; thus the highly variable surface emissivity and temperature, together with the temperature profile, bring further difficulties in aerosol remote sensing in the infrared. Then, the longwave domain is sensitive to particles in the coarse mode only, such as dust and volcanic aerosol, contrary to the shortwave where particles in the accumulation mode, emitted by biomass burning or industrial activities, can be observed.

However, the longwave domain has unique capabilities, such as night-time observations, or dust monitoring over deserts. The possibility to retrieve the altitude of the aerosol layer or its mineralogical composition is also of great interest. Next, only remote sensing in the longwave can bring accurate observations of infrared aerosol optical depths. Infrared instruments onboard meteorological satellite (e.g. Meteosat or NOAA satellite) give very long time series: extraction of a global climatology of aerosol from their observations provides very valuable information for climate studies. Furthemore, this domain is evolving very quickly, through the availability of new generation instruments, like the very high spectral resolution sounders AIRS or IASI.

The prospects for aerosol remote sensing in the infrared consist of the retrieval of microphysical information, and especially the mineralogical composition (e.g. quartz content in mineral dust particles). The synergy with visible observations also opens the way to innovating products, as both spectral domains are not sensitive to the same species of particles. For example, biomass burning plumes and mineral dust plumes can thus be disentangled.

Regarding the evaluation of aerosol direct radiative forcing, both the shortwave and longwave domain must be taken into account. Thus, the aerosol optical properties retrieved in the longwave are essential to estimate the total radiative impact at top-of-atmosphere and bottom-of-atmosphere. Concerning future applications of infrared retrieved aerosol properties, we foresee that their use in global climate models could constrain further the longwave part of aerosol direct forcing, which is far from being negligible.

Appendix: Conversion between wavenumber and wavelength

The wavenumber σ (in cm^{-1}) and the wavelength λ (in μm) are linked by the following relationship:

$$\sigma = \frac{10000}{\lambda}$$